OPTICAL RADIATIVE TRANSFER FEATURES OF DRY AND WET SOILS

A Dissertation

Presented to the Faculty of the Graduate School

of Cornell University

In Partial Fulfillment of the Requirements for the Degree of

Doctor of Philosophy

by

Jia Tian

May 2018

OPTICAL RADIATIVE TRANSFER FEATURES OF DRY AND WET SOILS

Jia Tian, Ph. D.

Cornell University 2018

Due to the importance of soil moisture in many fields of study, and given the sparsity of systematic research on radiative transfer features of moist soil in the optical domain, this dissertation focuses on both the spectral reflectance and transmittance features of dry and wet soils. In this work, the spectral reflectance and transmittance of soil are examined. The experiments lead to possible physical explanations for the spectral and directional features of reflectance spectra, and the results suggest how optical and proximal remote sensing might be useful in observations of soil moisture content.

The first experiment considered the change in spectral reflectance of soil samples during evaporative drying. The water absorption band depths at 970 nm and 1160 nm, in near infrared, decreased monotonically as the water content decreased, but they were not detectable in all samples; these water absorption bands will not be generally useful for observing surface soil moisture. In contrast, the band depths of the 1440 nm and 1930 nm absorption features were very responsive to the water content over the entire drying cycle. The change in band depth at 1930 nm was particularly interesting since the direction of the change reversed simultaneous with soil water evaporation rate change. A simple mathematical model suggests that the pattern of change in the band depth is related to the near extinction of light at the band center relative to the band shoulders.

The second experiment examined the degree to which light transmitted through quartz sand samples would maintain any directional characteristics. Transmittance decreased monotonically as the illumination angle increase, but slowly at all wavelengths. This indicates that directional radiation transmitted through the sand layer becomes diffuse with a millimeters-thin sand layer. For the saturated samples, the

influence of water on light transmittance in the VNIR (350-1300 nm) was the reverse of that in the SWIR (1330-2500 nm) wavelength region. In the VNIR, transmittance increased in the saturated sample relative to the dry sample, while transmittance decreased sharply after 1330 nm, with obvious spectral features characteristic of water absorption. Analysis of transmittance by quartz sand samples suggests that most of the directional variation due to the change in illumination angle can be attributed to surface reflective loss. The implication is that the directional reflection may be treated as a surface phenomenon, with the volume reflectance contributing a diffuse component.

The third experiment considered directional spectral reflectance of soil samples under dry and saturated conditions. When the samples were dry, the directional reflectance changed obviously with the phase angle, showing a stronger backward reflectance, while the forward reflectance was generally lower. For saturated soil samples, the directional characteristics of spectral reflectance apparent with dry soil were substantially reduced. In particular, the strong backward scattering weakened. Instead, the directional spectral reflectance became less sensitive to changes in both the illumination angle and the observation angle, especially for dark soils. Added water not only darkened the soil reflectance, but also eliminated the directional differences. This would make it difficult to discern soil structural properties when the soil moisture content is high.

BIOGRAPHICAL SKETCH

Jia Tian was born in a scholar family in Beijing, China. When Jia was in Beijing, her mother and grandparents gave her great influence on arts, especially on Chinese classical literature. Their acquaintance on literatures make Jia admire people who are experts in some domain and want to be a professor like them.

In her early teens, she moved to Nanjing with her parent. Nanjing was the capital city of six dynasties and is a city full of profound historical culture. The cultural atmosphere in Nanjing kept confirming Jia's inspiration on academic field. During that time, she found herself more talented in logical reasoning disciplines than arts and literature. As a result, she decided to focus on science and engineering as her father.

In 2008, Jia Tian was enrolled in School of Electronic Science and Engineering, Nanjing University, and was conferred bachelor degree of science four years later. In Nanjing University, she learnt how to focus on research and solve problems. Meanwhile, she felt that she was more attracted by disciplines related to nature. From her father's advice, she knew remote sensing, and was attracted by the combination of field experiments and laboratory processing.

Motivated by her interests in remote sensing and the desire to going academia, Jia continued her M.S./Ph.D. study in Cornell University majoring in Remote Sensing. Working with Professor William Philpot, Jia focused on soil water content research using hyperspectral methods.

谨以此献给我挚爱的家人和学生时代。

This work is dedicated to my beloved family and student time.

ACKNOWLEDGMENTS

Completing my Ph.D. study is one of the most significant events in my life. It is not only the end of my student life, but also the beginning of my brilliant career. Along the way till here, I would like to thank my family, my mentors, colleagues, and friends.

The most influencing people in my pursuit of scientific goals during study and work are my parents. They support me, encourage me, and comfort me. My father, as a professor, is so dedicated in his research that I was complaining about him spending too few time at home while I was a child. But as I am growing up, I realize that it is an enjoyment to have a career you really love and are willing to dedicate to. My mother, in contrast, spends more time in family. She was taking care of my life, and until today, I still cannot imagine how she was able to be so patient and careful to a self-willed child like me. All the good personalities I learnt are from them, and they are still telling me the world I had not reached yet. They are the role models I love, chase after, and will surpass eventually.

I'd like to thank my husband, Xiaodong. We never have a chance to meet in our homeland, but coincidence-by-coincidence made our life cross. He is smart, energetic, and trust-worthy. He always makes good plans in both life and work, and execute the plans precisely. Because of him, my Ph.D. life owns more happiness. For the next journey, let's walk together with holding hands.

I would like to thank my advisor, Professor William Philpot, for giving me unconditional support on my study. He introduced remote sensing to me, and guided me to scientific research. He showed me the charm of science as well as the dedication of a

researcher, and his effort gave me an unforgettable impression on insistence and earnestness.

I would like to thank my committee members, Professor Murray McBride and Professor Harry Stewart, who expanded my view. I learnt many related knowledge, which will help me in my further work. They let me know the relationship among different disciplines and gave me the potentials to solve problems from different aspects.

Last but not least, I really want to thank my friends in Cornell. We shared happiness and tears together; We joined the past and wish the best to the future of each other's life. Thank you for all your encouragement supporting me to continue my academic career in the future.

TABLE OF CONTENTS

LIST OF FIGURES

LIST OF TABLES

Introduction

Water darkens soil. This is apparent in the imprint of a receding wave on a beach, or in the drainage patterns in a drying field (Figure 1). What is less obvious is the reason for the darkening. Water is essentially transparent at visible wavelengths over distances of several meters (Pope and Fry 1997) allowing us to see brilliantly colored fish in aquaria and to determine the water depth in clear coastal waters (Philpot et al. 2004; Sinclair 2011). Given this clarity there can be no appreciable absorption of visible light by water over the distances light travels in the soil.

Figure 1: Drainage pattern in a plowed field in central New York, May 2013.

Darkening in the visible, then, must be due primarily to absorption by the soil, enhanced by the presence of water. By altering the relative index of refraction at the particle surface, water reduces reflectance, increases the probability of absorption by the particle, and enhances the probability of light being scattered forward, deeper into the soil. This will occur even when water is simply adsorbed to the soil particles. The tendency for increased scattering of light – and the increased probability of absorption by the soil particles – is further enhanced by the presence of air-water boundaries in the pore spaces of the soil.

Refraction effects are also important in the near infrared (NIR; 0.7-1.0 μm) and shortwave infrared (SWIR; 1.0-2.5 μm), but darkening in the SWIR – particularly at wavelengths beyond 1350 nm – is primarily due to absorption by water. The absorption coefficient of water increases by several orders of magnitude from the visible to the SWIR, and includes several pronounced absorption bands that are readily apparent in reflectance spectra of wetted soils (Lobell and Asner 2002). These features are often the focus of attempts to estimate soil moisture content using reflectance (Demattê et al. 2006). Absorption by water clearly has a major impact on the darkening at these wavelengths, even though the optical path through water may be only tens of microns.

The interplay of standing water, adsorbed water, pore water and the different configurations of soil-water, soil-air, and air-water interfaces all contribute to the changes in spectral reflectance of soils. These vary not only with water content, but also with the size and distribution of the pore spaces, the particle size distribution, the compaction of the soil, and even the mix of hydrophilic vs. hydrophobic surfaces in the soil. Such complexities have confounded attempts to find simple relationships between soil reflectance and soil moisture.

The objective of this work is to explore how soil moisture influences the spectral and directional character of reflectance. The effects of wetting on soil reflectance and transmittance are studied, and viewed with different illumination and observation angles. The ultimate goal is to develop a practical model that describes the reflectance in terms of soil content and structure.

Literature Review

Soil moisture has been studied for many decades because it is a fundamental property that is important in many fields of study, such as hydrology, meteorology and agronomy (Oki and Kanae, 2006). For applications in which moisture at or near the surface is important (e.g., agronomy), there are a variety of techniques that have been developed to measure soil moisture including both probe-related ground measurements and remote sensing methods. The ground-based methods are the proven, reference observations, but remote sensing techniques hold promise for providing more extensive areal and temporal observations.

1.1 Ground measurements

There are many ground-based techniques for measuring soil moisture in the field, including time-domain reflectometry (TDR) (Jones et al., 2002), frequency domain sensors (Gaskin and Miller, 1996), electrical resistivity tomography (Ozcep et al., 2009), and ground penetrating radar (Galagedara et al., 2005) etc. Most of these methods are effective with larger soil volumes and are not as useful for characterizing surface moisture (Zhu et al., 2010).

Ground measurements usually provide data that are easily calibrated, but each measurement only applies to a single, small area. They are easily adapted to monitoring temporal variations (Parent et al., 2006), but are difficult to use to map spatial variations. The most prominent advantage of the ground-based measurements is in providing soil moisture content at root-zone depth, the most appropriate range for agricultural studies.

1.2 Microwave remote sensing

Microwave remote sensing systems may be either active or passive. Active (radar) systems transmit an electromagnetic pulse and measure the backscattered energy, while passive radiometers observe the energy emitted from the target itself (Ulaby et al., 1982). Microwave remote sensing has the general advantage of being unaffected by cloud cover and not requiring solar illumination. This all-weather capability is particularly true for systems that operate in the low frequency microwave range (1 – 10 GHz) (Njoku and Rague, 1996; Wagner et al., 2006).

For a number of years, microwave remote sensing methods have been the main focus of research aimed at retrieving the moisture content of the top several centimeters of soil (Albergel et al., 2008; Ford et al., 2014; Sabater et al., 2007; Walker et al., 2001). Sabater et al. (2006) also studied four data processing methods. The overall result of their study indicates that all four methods yield satisfactory results, which suggests that retrieving root-zone soil moisture content from surface soil water content is feasible.

Soil moisture content most strongly affects passive microwave radiation from soils due to the difference between the dielectric constant of water (~80 at frequencies below 5GHz) and that of dry soil (~3.5) (Njoku and Entekhabi, 1996); the soil dielectric constant increases with increasing water content. However, the measurement of radiation is also influenced by soil surface roughness (Choudhury et al., 1979; Mo et al., 1987; Tsang and Newton, 1982), attenuation and emission by vegetation cover (Jackson, 1982; Jackson and Schmugge, 1991; Pampaloni and Paloscia, 1986), and surface and subsurface heterogeneity (Kerr and Njoku, 1990; Tsang et al., 1975; Wilheit, 1978). The most recent global soil moisture measurement is provided by the Soil Moisture Active

Passive (SMAP) satellite mission. SMAP was launched on January 31, 2015, and one of its objectives is to measure the amount of water in the top 5 cm of soil of the Earth. Compared to optical remote sensing, SMAP is able to estimate deeper soil moisture content by integration every 2 to 3 days. However, microwave systems like SMAP can only provide data on the landscape scale (kilometers to 10s of kilometers). They are incapable of finer, field-level observations. Microwave systems are also not readily adaptable to ground observations or for monitoring evaporation.

1.3 Surface soil moisture – root-zone soil moisture

Soil moisture content, as studied in agriculture, is normally required over large areas. However, the difficulty and expense of ground measurements makes it problematic to collect measurements at multiple sites or even frequent observations at a single location. Because of the inconvenience of direct root-zone soil moisture measurements, other, more easy-obtained parameters are often used for moisture estimates. For example, Mahfouf (1991), reasoning that the near-surface temperature and humidity are influenced by the soil moisture, developed a model to describe the effect and then, inverting the model, used the above-surface measurements to retrieve the soil moisture in root-zone measured using neutron sounding (soil-water profile) and gypsum blocks (first 5 cm of the soil). Although the results showed promise, the link between air temperature/humidity and root-zone soil moisture is rather indirect and imprecise.

Surface soil moisture may be more reliably related to the root-zone soil moisture content. For a number of years, microwave remote sensing methods have been the main focus of research aimed at retrieving the moisture content of the top several centimeters of soil (Albergel et al., 2008; Ford et al., 2014; Sabater et al., 2007; Walker et al., 2001).

Sabater et al. (2006) also studied four data processing methods. The overall result of their study indicates all four methods yield satisfactory results, which suggests that retrieving root-zone soil moisture content from surface soil water content is feasible.

1.4 Evaporation

Evaporation is a key hydrologic driver that directly connects the transition of surface soil moisture (liquid) to vapor, and the soil surface is exactly where this process occurs. Direct soil evaporation and plant transpiration consume 20% and 40% of the terrestrial precipitation, respectively (Oki and Kanae, 2006; Shahraeeni and Or, 2012). Sherwood (1929) pointed out that, at the beginning of drying process, very wet solids exhibit a period with a constant rate of drying and that, after achieving a critical liquid content, the rate of drying starts to decrease. These two periods are called constant rate period (stage-I) and falling rate period (stage-II). The constant rate period is supported by internal capillary flow (Van Brakel and Heertjes, 1978; Yiotis et al., 2006). For the constant rate period, water in the near-surface is driven by capillary flow moving water to the surface so that the rate of drying by evaporation can continue at a constant rate. For the falling rate period, disruption of hydraulic continuity between the primary drying front and the evaporating surface leads to the rate change. The rate of evaporation is another indicator for water content, and appears to be observable using spectral changes in the water absorption bands derived from optical remote sensing.

1.5 Other soil characteristics

Some soil characteristics (e.g. pore size) influence the evaporative process (Lehmann and Or, 2009), as well as spectral reflectance features in remote sensing, so researchers usually classify soil samples for comparison (Lobell and Asner, 2002; Njoku

and Entekhabi, 1996). In laboratory experiments, samples can be classified based on varied soil sources, e.g., artificial soil samples, soil core samples, and surface soil samples (Zhu et al., 2010). Similarly, based on different spectral features, soil samples were sorted into organic matter-rich, lime-rich, and iron oxide-rich (Lesaignoux et al., 2010). For in situ soil samples, they could be labeled just by soil order in USA soil taxonomy (Lobell and Asner, 2002). In other studies, soil samples might be described based on their different material contents (Liu et al., 2002), or color (Lesaignoux et al., 2013).

1.6 Optical remote sensing: reflectance in the solar domain

There are many studies that have drawn a connection between soil moisture and the reflection from soil surfaces in the visible/near infrared (VNIR) and the shortwave infrared (SWIR) spectral regions (Ahmad et al., 2011; Kaleita et al., 2005). A distinct problem with drawing a relationship between reflectance and soil moisture (as defined for agricultural or hydrological purposes) is that optical radiation does not penetrate soil beyond the surface layer; the reflectance derives only from the first several millimeters of soil at most (Liang, 1997).

To study the relationship between soil reflectance in the optical domain (400 - 2500 nm) and soil moisture, usually several wavebands are selected by some form of optimization method to indicate reflectance changes for a particular set of soil samples. Typically, a linear forward stepwise regression technique will be used for the optimization. For example, Liu et al. (2002) determined an optimal band set that included 1400, 986, 1998, 574, 2189, 1672, and 450 nm. In another study (Lobell and Asner, 2002), a single wavelength, 2200 nm, was selected based on its absorption

response in mineral soils, and 600 nm and 1200 nm were included for contrast. Different studies also take a different approach to calibration and normalization. For example, Lobell and Asner's (2002) results were based on absolute reflectance, while Liu (2002) focused on normalized reflectance, i.e., dividing the reflectance from a wet soil by the reflectance of the same type of soil when it was dry. This minimizes variations due to roughness and sensor-source geometry effects (Baret et al., 1993).

1.7 Existing Models

In order to estimate the soil moisture content from spectral reflectance in the optical domain, researchers usually rely on empirical rather than physically-based models. A typical approach is to employ an exponential model describing the relationship between spectral reflectance in optical domain and soil moisture content (Lobell and Asner, 2002; Zhu et al., 2010), but a combination of linear and nonlinear functions has also been proposed, as has an empirical model that relies on a polynomial relationship (Lesaignoux et al., 2010). In Bach and Mauser's (1994) research, two processes are taken into account. One is the general darkening of soil due to internal reflection in a water layer and the other one is absorption of water contained in soil at certain wavelengths. Besides studies on relationship between absolute reflectance value and soil water content, a soil moisture retrieval model was built with transformed reflectance based on the Kubelka-Munk two-flux radiative transfer theory (Sadeghi et al., 2015). Sadeghi's model is verified using laboratory-measured spectral reflectance data of different soils (from Lobell & Asner 2002; Whiting et al. 2004).

All of these studies focus on patterns of change in reflectance with changing water content. Most studies showed the spectral reflectance decreasing with increasing soil

moisture content (Chang et al., 2005; Lesaignoux et al., 2013; Planet, 1970; Stoner and Baumgardner, 1981; Zhu et al., 2010). A few studies have indicated that high soil moisture content would sometimes enhance the spectral reflectance (Liu et al., 2002; Neema et al., 1987), and that the critical point at which reflectance began to increase with increasing soil moisture content occurred at different moisture levels for different kinds of soil (Liu et al., 2002). The inversion may be caused by specular reflectance of water film covering soil surface from over saturation (Sadeghi et al., 2015).

All of the existing research results indicate that the SWIR region is more sensitive than the VNIR for mapping the relationship between spectral reflectance from soil surface and soil moisture content (Lobell and Asner, 2002; Zhu et al., 2010). The sensitivity of reflectance in the SWIR to soil water content is directly related to the wavelength-dependent water absorption coefficient. Figure 2 shows the variability of the water absorption coefficient in the optical domain. In VNIR region, the small absorption coefficient indicates that water is relative transparent, whereas, water is strongly absorbing in SWIR region. Lobell and Asner (2002) note that reflectance in the SWIR region is responsive to a wider range of soil moisture - up to 50% of the volumetric water content - while the reflectance in VNIR region can reach a minimum when soil moisture content is only about 20%. They also note that the uncertainly in the estimate of soil moisture content based on SWIR observations was only half the uncertainty for similar estimates based on observations in the VNIR region. However, in a similar study, (Liu et al., 2002) concludes that the shorter wavebands could be more efficient for the estimate at hard-to-estimate, high moisture levels.

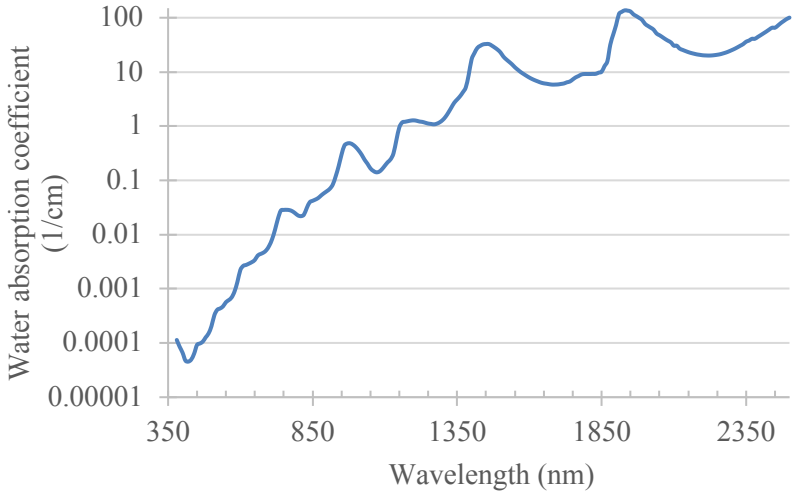

Figure 2: water absorption coefficient from 380 to 2500 nm in logarithmic scale.

Another approach is that taken by Whiting et al. (2004), who empirically fit Gaussian functions to normalized reflectance spectra. Their model was particularly sensitive to soil type and operated most effectively when applied to unsaturated samples. Other empirical models, while very effective on a limited range of soil types, have also demonstrated a strong sensitivity to specific soil characteristics. Even when derived from hyperspectral data, most of the empirical models make use of a reduced set of wavelengths (Khanna et al., 2007; Zhang et al., 2003), or a set of basis vectors (Janik et al., 2009; Lesaignoux et al., 2013), and tend to be less generally effective.

1.8 Optical remote sensing: transmittance in the solar domain

Transmittance of sunlight into soil is a significant issue for both practical problems and theoretical studies. In agricultural applications, the penetration depth of UV, visible and near-infrared (VNIR) radiation into the soil is important for promoting the germination of seeds. Appropriately, transmittance measurements have generally been limited to the VNIR. Particular attention has been given to the 290-500 nm range, which

is important for quantification of chemical and biological processes such as photochemical transformation of pesticides or other organic compounds (Balmer et al., 2000; Hebert and Miller, 1990), while 660-730 nm radiation influences seed germination (Benvenuti, 1995; Bliss and Smith, 1985; Woolley and Stoller, 1978).

Transmittance is also related to the depth at which the measured reflectance signal originates – the information depth (Ciani et al., 2005). As such, it is particularly useful in identifying the soil characteristics that contribute to reflectance, and can inform radiative transfer modeling (Banninger et al., 2004; Ciani et al., 2005; Philips-Invernizzi et al., 2001). Fenchel and Staarup (1971) found that the penetration depth was very sensitive to the particle size distribution, and was rather strongly wavelength dependent in rinsed quartz sand (Fenchel and Straarup, 1971). Woolley and Stoller (1978) found very strong wavelength dependence in the transmittance of a sand sample relative to that of a silty clay loam. Other studies have shown that penetration is deeper at longer VNIR wavelengths, and that particle size distribution influences the light penetration (Bliss and Smith, 1985; Haardt and Nielsen, 1980). Explicitly, Bliss and Smith (1985) found that transmittance decreased sharply as the size of the sand particles decreased. Neema et al. (1987) reported and modeled data from Shah (1981) indicating that transmittance of visible light initially increased with moisture content, but then decreased as the pore spaces filled, a finding not noted elsewhere. Recent work has focused on the directional character of reflectance, i.e., the Bidirectional Reflectance Distribution Function (BRDF) (Bachmann et al., 2014; Baranoski et al., 2014). Given the sensitivity of the BRDF to the structure of the soil (e.g., density, pore space, particle

size), this work suggests that there would also be a directional character to the transmitted radiation.

1.9 Bidirectional reflectance directional function (BRDF)

A consistent conclusion reached in validating the models considered above is that the models are most effective when adapted to a limited range of soil types. This is likely due to the fact that the empirical models do not explicitly incorporate effects of particle size, pore size, and surface roughness. Bi-directional reflectance measurements, on the other hand, are particularly sensitive to such characteristics (Bachmann et al., 2014; Cierniewski et al., 2010; Wang et al., 2010; Wassenaar et al., 2005). There are a number of modeling approaches to describe such observations, ranging from formal, physically exact approaches (Mishchenko, 2011), to highly approximate representations of the surface (Banninger et al., 2004; Cierniewski et al., 2004). So far, only one bi-directional model (Voss and Zhang, 2007; Zhang and Voss, 2006), has directly addressed the effect of water on reflectance and that model considered only dry, saturated and submerged conditions – not unsaturated soils. They noted that the BRDF of saturated, particulate layers becomes more Lambertian as the liquid becomes more absorbing, and state that the relationship can be modeled by a two-part empirical model, with one part describing reflectance from the front surface and another part describing reflectance from the bulk material. In a review of models of bi-directional reflectance, Zhang & Voss (2008), consider the BRDF from saturated sands using pore liquids with different refractive indices. The particles ranged from black to bright, translucent grains. They noted that, even for observations at visible wavelengths, the BRDF and plane albedo of saturated samples couldn't be attributed solely to the relative index of refraction, and indicated

that the percentage of translucent particles and the roughness of individual particles is also a concern.

The primary focus of the bi-directional reflectance models is on the geometric aspects of the scattering from particulate surfaces and they are generally designed to handle variations in roughness, density and porosity; however, the index of refraction of the medium is a spatial constant and the index of refraction of the particles is also assumed to be constant. There is no built-in mechanism to differentiate between air and water in the pore spaces, yet a model capable of describing the directional characteristics of reflectance would be more likely to succeed in capturing the effects of moisture, if an appropriate adaptation can be found.

CHAPTER 2: Relationship between surface soil water content, evaporation rate, and water absorption band depths in SWIR reflectance spectra

2.1 Introduction

Soil moisture is a key factor for many fields of study, ranging from hydrology and agronomy to meteorology (Wigneron et al., 1998). The most commonly used methods for soil water content measurements are ground-based techniques (time-domain reflectometry, frequency domain sensors, etc.) and microwave remote sensing. The disadvantages of these methods are as obvious as their strengths. Ground measurements can provide data that are easily calibrated, but each measurement only applies to a single, small area. While they are easily adapted to monitoring temporal variations (Parent et al., 2006), they are difficult to use to map spatial variations. Microwave radiation can penetrate into soil and microwave remote sensing is widely used for soil monitoring, but the spatial resolution is relatively coarse even for airborne systems (Hasan et al., 2014), the penetration is strongly influenced by soil water content, and the penetrating depth decreases dramatically with increasing water content (Njoku and Rague, 1996). Thermal sensing has also been brought to bear on the problem of moisture sensing, based on the change in emissivity of wet soil, usually in combination with an optical sensor capable of providing a vegetation index (e.g., Sandholt et al. 2002).While this approach has the distinct advantage of providing an estimate of soil moisture even in the presence of vegetation, it is an approximate measure, most useful when applied to relatively large areas.

Optical remote sensing also has advantages and disadvantages. Radiation in the visible/near infrared (VNIR) and shortwave infrared (SWIR) does not penetrate into the soil beyond the surface layer, with reflectance deriving from the first several millimeters of soil at most (Ciani et al., 2005; Liang, 1997; Tester and Morris, 1987; Zhang et al., 2003). In spite of the shallow penetration, changes in reflectance are commonly related to volumetric changes in soil water content (Leu, 1977; Lobell and Asner, 2002; Nolet et al., 2014; Sadeghi et al., 2015; Whiting et al., 2004). The limited penetration is balanced by the capacity to make observations at high spatial resolution over large areas (Nolet et al., 2014). Even the restriction to surface measurements has a positive side; it is at the surface where evaporation occurs. Soil evaporation is a key process which accounts for 20% of the terrestrial precipitation; optical remote sensing might provide a window into the evaporation state (Oki and Kanae, 2006; Zhang and Voss, 2006).

The presence of moisture greatly influences spectral reflectance in both the VNIR and SWIR, especially in the major water absorption bands. Broadly speaking, reflectance decreases with increasing water content with the effect being more pronounced at longer wavelengths (SWIR). Exceptions to this trend have been noted – particularly when approaching saturation (Liu et al., 2002) – and may be modeled by taking Fresnel reflectance into account (Sadeghi et al., 2015). Many researchers have observed the change in the spectral reflectance of soils due to moisture, and some have found empirical, predictive relationships with spectral reflectance values, but these are generally influenced by soil type, and are biased by the reflectance of the dry sample (Haubrock et al., 2008). Some generalization appears to be possible; for example Sadeghi et al. (2015) were able to find general relationships for three broad groups of

soil types. However, the physical link between soil type, water content and spectral reflectance remains an unsolved problem. Interestingly, Small et al. (2009) observed a change in reflectance that varied with the drying rate, and noted that the soil moisture and particle size distribution appeared to be separable in the reflectance spectra. This suggests that there might be a spectral measurement that would be sensitive to the moisture content and insensitive to soil type.

In this paper we begin with the premise that there is a spectral feature that will be sensitive to soil moisture while being insensitive to other soil characteristic (particle size distribution, composition, etc.). An obvious place to start is with the strong water absorption bands in the infrared, since these will respond primarily to changes in water content, and would reasonably be expected to do so independently of soil type. Following the procedure of Small et al. (2009) we focus on the change in reflectance and its relationship to the drying rate of the soil. The depth of water absorption bands is used since it is expected to be directly related to the surface soil water content and is less likely to be sensitive to the magnitude of the soil reflectance. Using the band depth as a metric, the response of water absorption bands in the SWIR region to the soil water content for three distinct soil types are observed, described and related to the evaporation rate and the drying state of the soil.

2.2 Experimental Design

2.2.1 Samples

Three soil samples (Table 1) were observed in the experiments: a white quartz sand, masonry sand, and a typical Ithaca-area soil. Based on the particle size distribution, the samples were classified into three texture groups.

Table 1. Soil physical characteristics

	quartz sand	Masonry sand	Ithaca soil
Very coarse and coarse sand	86.1%	18.3%	3.8%
Medium sand	10.1%	27.0%	
Fine and very fine sand	3.8%	48.4%	
Silt	0 %	4.4 %	77.0 %
Clay	0 %	1.9 %	19.2 %
Texture*	Coarse sand	Sand	Silty loam
Organic matter	0%	0.2%	5.3%
Bulk density	1.44 g cm^{-3}	1.53 g cm^{-3}	0.95 g cm^{-3}

* Texture classification is based on USDA standard.

2.2.2 Experimental setup and procedure

Figure 3 illustrates the experimental setup. The spectrometer was an ASD FieldSpec® Pro with a spectral range of 350-2500 nm. The spectral resolution is ranging from 3 nm in the visible to 12 nm at 2100 nm, and with a sampling interval of 1 nm. The ASD fiber optic probe was fitted with an 8° field of view (FOV) fore optic and mounted 18 cm above the sample (nadir view). The sample holder was a 1.2 cm tall black plastic cylinder with a 5.1 cm inner diameter and a sieve bottom. The sieve bottom allowed water to be drawn up into the sample by capillary action, minimizing disturbance of the soil surface. The volume of the sample holder was then 24.5 cm^3. Illumination was provided by an ASD Pro Lamp, a 70 watt quartz-tungsten-halogen light source designed to provide stable illumination over the 350 to 2500 nm range. Reflectance was determined by measuring the radiance from the sample relative to a calibrated, white (99% reflectance) Spectralon® standard panel.

The sample holder was filled with dry soil, and the surface was leveled with a metal straight edge in order to provide a uniform surface with no preferred orientation. Observation of reflectance collected while rotating the sample holder in 90° increments produced no discernible change in reflectance. For the duration of the experiment, the sample holder sat on a scale (Ohaus SP200) with an accuracy of 0.01g, which was linked to a computer via a USB connection. The scale was programmed to report the weight once each minute. Spectra were collected at 5 minute intervals.

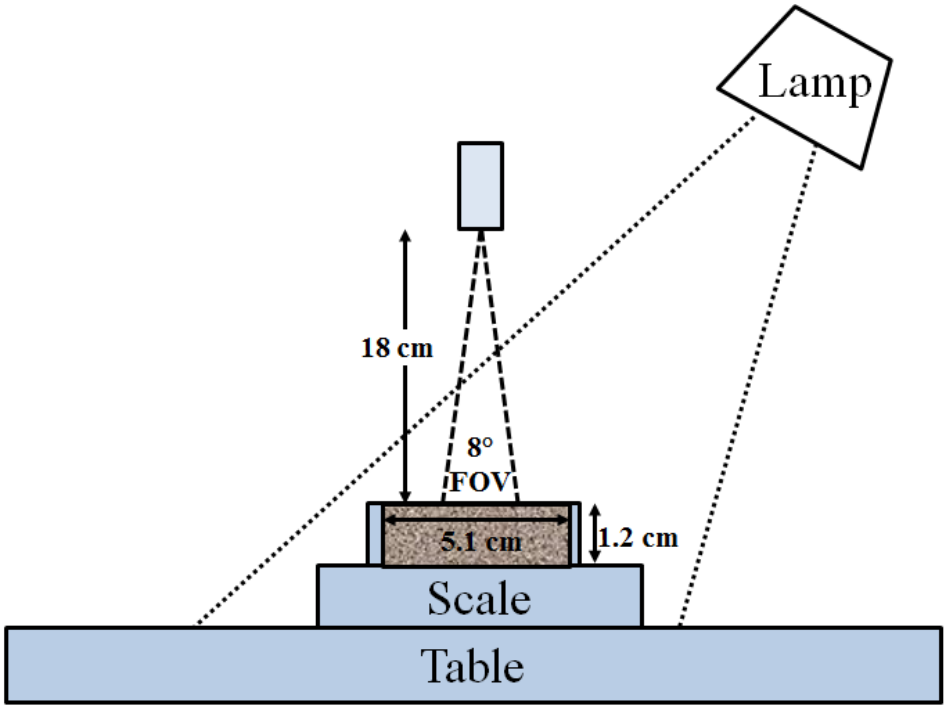

Figure 3: Sketch of experimental setup.

Reflectance from soil is very much a surface phenomenon in that the reflected light derives from the first few millimeters of the soil surface. Small changes in the near-surface structure (e.g., a change in the size or density of the pore spaces) can alter the reflectance. Thus, rather than wetting the sample from the top, the filled sample holder was placed on a saturated sponge and the soil then drew up the water through the sieve

bottom via capillary action. This procedure minimized disturbance of the sample surface and insured maximum saturation.

2.2.3 Methodology

The experiment was designed to observe the dynamic correlation between soil water content and spectral reflectance. Based on the premise that the particle size and pore space distribution would have the most significant effect on the rate of evaporation and water retention characteristics, three soil samples were selected to span a wide range of soil characteristics (Table 1). Water content was monitored based on sample weight, and the depth of the most prominent water absorption bands was used as the metric. The working hypothesis was that the depth of the absorption bands, being a direct measure of the amount of water encountered by the reflected light, would be less sensitive to the specific soil type, and would be most likely to relate directly to the water content.

Selection of the absorption bands was based on the absorption spectrum of water (Figure 4). Water is essentially transparent in the visible over the optical path lengths typical for soil; however, absorption increases dramatically throughout the infrared. In the SWIR, absorption is strong enough that, at the center of the major absorption band (1930 nm), virtually all the light can be absorbed over very short optical paths (~200 μm). For the weaker absorption bands (970 nm, 1160 nm) absorption may not even be apparent until after relatively long distance (millimeters), and complete extinction would be unlikely in soils.

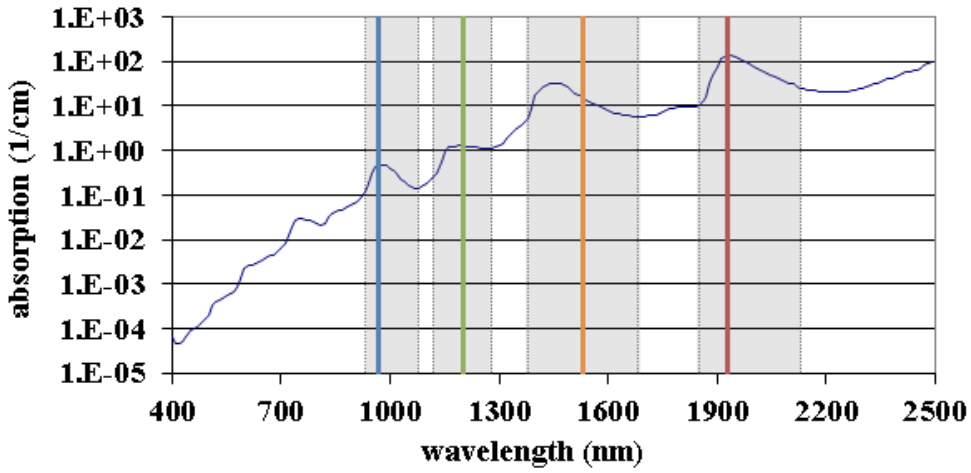

Figure 4: Absorption spectrum of water (Kou et al., 1993; Pope and Fry, 1997). The center wavelengths (970 nm, 1160 nm, 1440 nm and 1930 nm) of the major absorption bands are marked with vertical, solid lines. The shoulders of the bands are indicated by the boundaries of the gray areas.

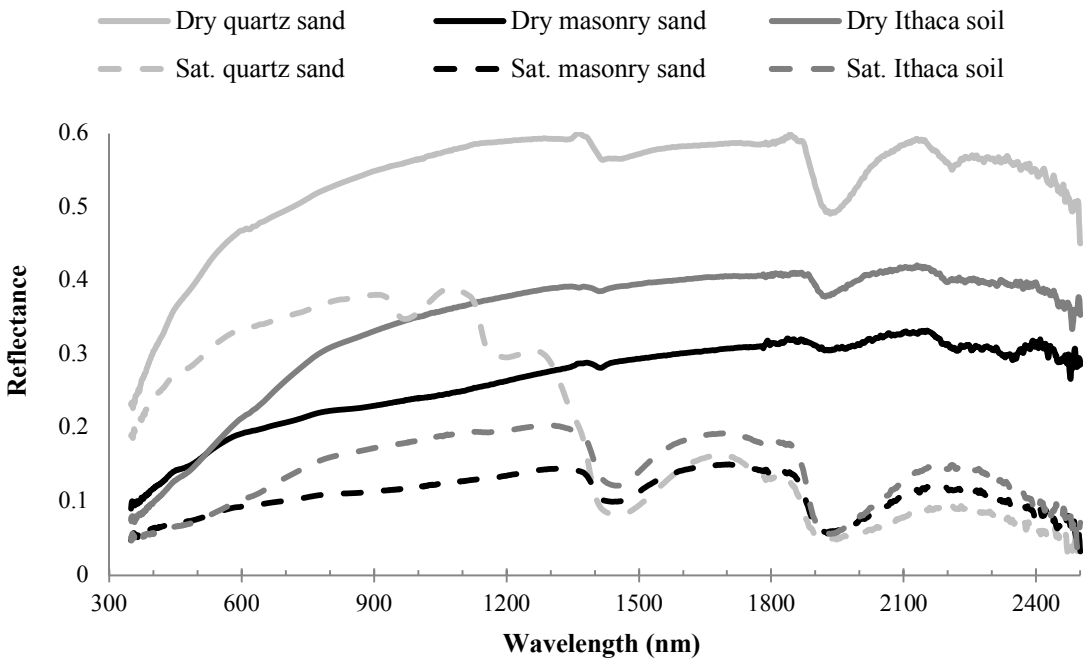

Figure 5: Spectral reflectance curves of air-dried and saturated soil samples (light gray for quartz sand, black for masonry sand, and medium gray for Ithaca soil).

Figure 5 shows the spectral reflectance curves of air-dried and saturated samples of each of the soils. The quartz sand is highly reflective and translucent, with large particles and a relatively narrow size distribution; the reflectance of the dry masonry

sand and the Ithaca soil are darker at all wavelengths than the quartz sand. The two darker soils are similar in the visible, but differ markedly in the NIR and SWIR where the masonry sand is much less reflective. Both the masonry and Ithaca soils consisted of smaller particles than the quartz sand and both had a relatively wide size distribution. All three air-dry spectra exhibit absorption features centered near 1440 nm and 1930 nm. Based on both its location and breadth, the 1930 nm feature is almost certainly a water absorption feature meaning that there is still some water present in the air-dried samples. While a mineral absorption feature at 1440 nm is common (Clark, 1983), the presence of the 1930 nm absorption feature suggests that the 1440 nm band is also due to the presence of water (Clark et al., 1990).

Reflectance spectra of the saturated samples (Figure 5) are darker at all wavelengths than their dry counterparts. All four major water absorption features are visible in the spectrum of the saturated quartz sand while only the strongest absorption bands at 1440 nm and 1930 nm are apparent in the reflectance spectra of the darker soils. Note that the reflectance of the quartz sand dips below the reflectance for the dark soils through most of the SWIR, although the reflectance at shorter wavelengths remains substantially higher. This is consistent with a longer optical path length through water for the light reflected from the quartz sand. Interestingly, the water absorption bands at 970 nm and 1160 nm only appear in the quartz sand spectrum, in spite of the fact that all three soils darken significantly with increasing water content. This, too, would be consistent with a substantially longer water optical path for light in the quartz sand. Possibly this is related to the fact that the quartz particles were translucent and there was a higher probability of light penetrating through the particles.

Table 2. Selected water absorption bands in SWIR region

No.	Left shoulder	Band center	Right shoulder
I	930 nm	970 nm	1080 nm
II	1120 nm	1160 nm	1280 nm
III	1380 nm	1440 nm	1680 nm
IV	1850 nm	1930 nm	2130 nm

2.2.4 Absorption Band depth

In hyperspectral remote sensing, the depth of an absorption band of a target material is commonly used as an indicator of the amount of that material present within a host material. When absorption by the target material is negligible away from the center of the absorption band, a normalized absorption band depth is recommended in order to minimize the effect of the differences in reflectance of different host materials (Clark and Roush, 1984). With water, however, absorption is strong throughout the infrared and is extreme in the SWIR. Absorption at these wavelengths by the host material (soil) is negligible; the band depth registers the spectral difference in attenuation of water at the band center and the band shoulders. For wet soil, then, a simple difference measure of the band depth is appropriate, and is likely provide more consistent information than either simple reflectance or a normalized band depth. A simple estimation of band depth is given by the vertical distance from the minimum reflectance to a straight line connecting the shoulders of the water absorption feature (Lobell and Asner, 2002; Morris et al., 1982). The interpolated reflectance, R_{int} , on the connecting line at the center wavelength is given by:

$$R_{int} = \frac{R_{left} - R_{right}}{\lambda_{left} - \lambda_{right}} * \left(\lambda_{center} - \lambda_{left}\right) + R_{left} \quad , \tag{1}$$

The band depth, ΔR_c, is then simply

$$\Delta R_c = R_{int} - R_c \, , \tag{2}$$

where R_c is the reflectance at the band center, illustrated in Figure 6. The central and shoulder wavelengths for the four absorption bands are listed in Table 2 and illustrated in Figure 4. The selection of shoulder wavelengths was based on the shape of the dry sample curves for the 1440 nm and 1930 nm bands, while the shoulder wavelengths for the 970 nm and 1160 nm bands and the central wavelengths for all bands were determined from minima of the saturated sample curves.

2.2.5 Water content and evaporation rate

Volumetric water content (VWC) was selected as the indicator of water content. Equation (3) shows the VWC calculation,

$$\text{VWC} = \frac{m_{water}}{\rho_{water} \cdot V_{total}} \quad , \tag{3}$$

where m_{water} is the mass of the water, ρ_{water} is water density (1.0 g/cm^3), and V_{total} is total volume of solids, water, and air space. Water loss was due entirely to evaporation at the soil surface and is the link between the spectral features and water content. The rate of evaporation was calculated as the mass change per unit time.

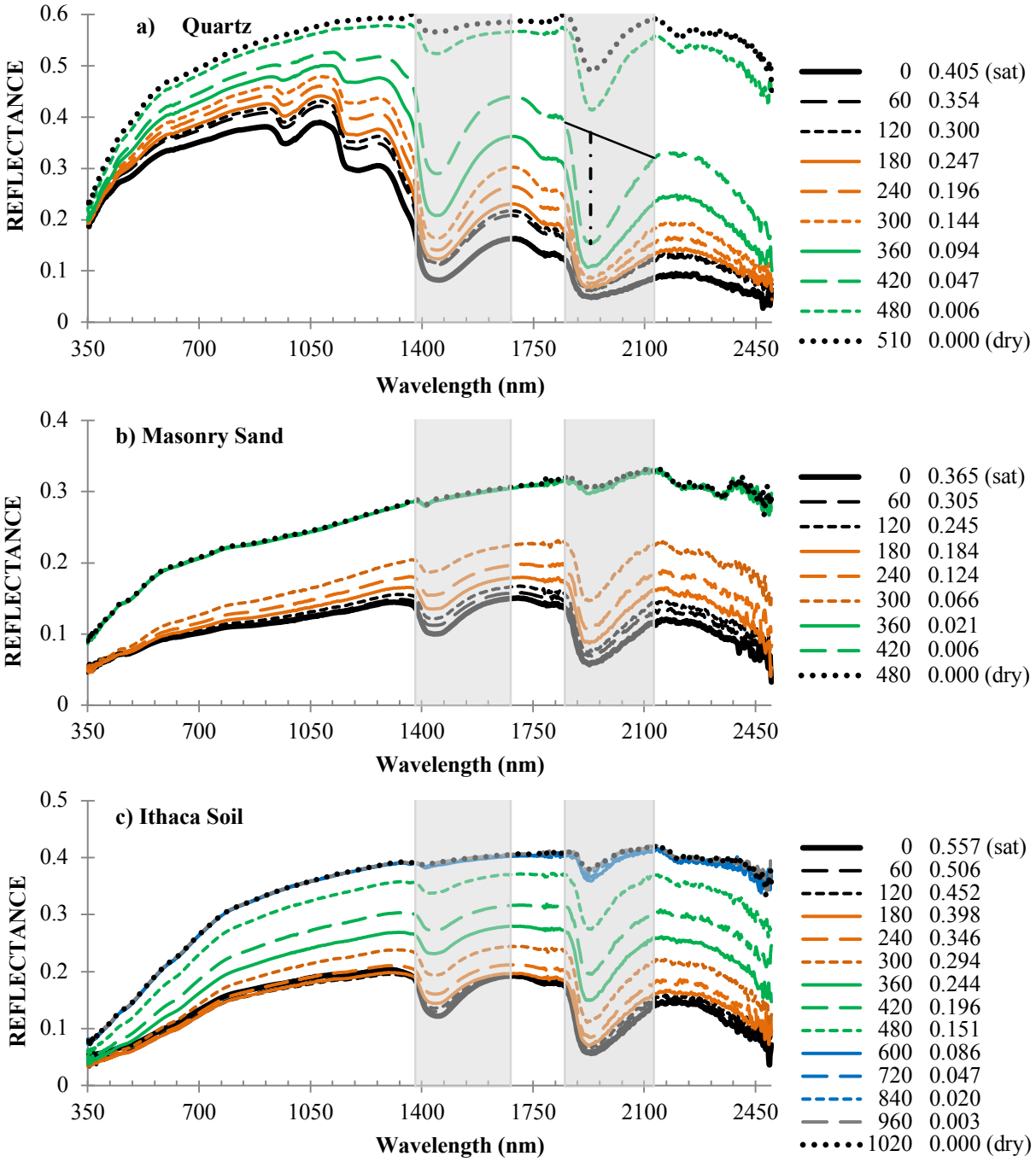

Figure 6: Spectral reflectance changes with changing water content from saturated to air-dry. The time interval between spectra is 60 minutes (120 min for the last six hours for the Ithaca soil). Grey strips mark the major absorption bands; the dash-dotted line at 1930 nm indicates the interpolated band depth, R_c; a) quartz sand dried for 510 minutes, b) masonry sand dried for 480 minutes, and c) Ithaca soil dried for 1020 minutes, shrinking significantly during the late stage drying.

2.3 Results

Spectra collected at hourly intervals during the drying process are shown in Figure 6 for all three soil types. Reflectance is highest when the soils are dry, with reflectance in the infrared being higher than in the visible. As water content increases, reflectance decreases at all wavelengths, but the decrease is much more pronounced in the infrared, especially at the major water absorption bands at 1440 nm and 1930 nm. The weaker water absorption bands at 970 nm and 1160 nm are only visible in the quartz sand spectra (Figure 6a).

There are some features in the reflectance spectra that are consistent for all three soils during the drying process: 1) the change in reflectance is more pronounced at longer wavelengths, 2) the change in reflectance is more dramatic at the 1440 nm and 1930 nm water absorption bands than at other wavelengths, 3) the 1930 nm absorption band is always deeper than 1440 nm band, and 4) reflectance change is slow during the first few hours of the drying period, becomes more rapid, and then slows again toward the end of the period. Other features in the reflectance spectra are not as consistent among the three soils. For example, two lesser water absorption features appear in the saturated quartz sand reflectance at 970 nm and 1160 nm, but are notably missing in the saturated reflectance spectra for the other two soils. The sequence of changes in reflectance also differs greatly among the three soils. Reflectance of the quartz sand increases in the first 60 minutes of drying, stabilizes for about an hour, and then increases steadily for the next four hours until near the end of the drying period when reflectance increases sharply. The masonry sand reflectance increase begins slowly, but accelerates over the first four hours and then increases abruptly, reaching what is very

nearly the dry reflectance except for the water absorption band at 1930 nm. The Ithaca soil reflectance remains quite dark for the first four hours – essentially unchanged from the saturation level – and then increases steadily over a period of five hours, reaching the level of dry reflectance everywhere but at the water absorption band at 1930 nm. (Similar patterns were documented by Small et al. (Small et al., 2009) for a much larger range of soils.) The strong change in the SWIR absorption bands and the persistence of change when the soils are nearly dry suggest that they will be the most effective features for characterizing water content of the samples, especially during the final drying stages.

2.3.1 Change in Band depth over the drying cycle

The change in band depth over the full drying period for all four absorption bands and for each of the three test soils, along with the change in VWC is shown in Figure 7. For all three soils, the change in VWC is nearly linear until the very end of the drying period indicating a constant evaporation rate typical of soils drying under constant temperature and humidity (Schindler and Müller, 2006). For the quartz sand, the band depths for the weaker absorption bands (970 nm and 1160 nm) decrease monotonically with time, coincident with the decrease in VWC. The change in band depth is slight for the first 200 minutes, but changes somewhat more rapidly as the sample dries. For the masonry sand and Ithaca soil, the 970 nm and 1160 nm bands are not readily apparent and change in band depths is negligible. This is consistent with earlier observations (Knadel et al., 2014; Lesaignoux et al., 2013; Lobell and Asner, 2002; Nolet et al., 2014; Small et al., 2009).

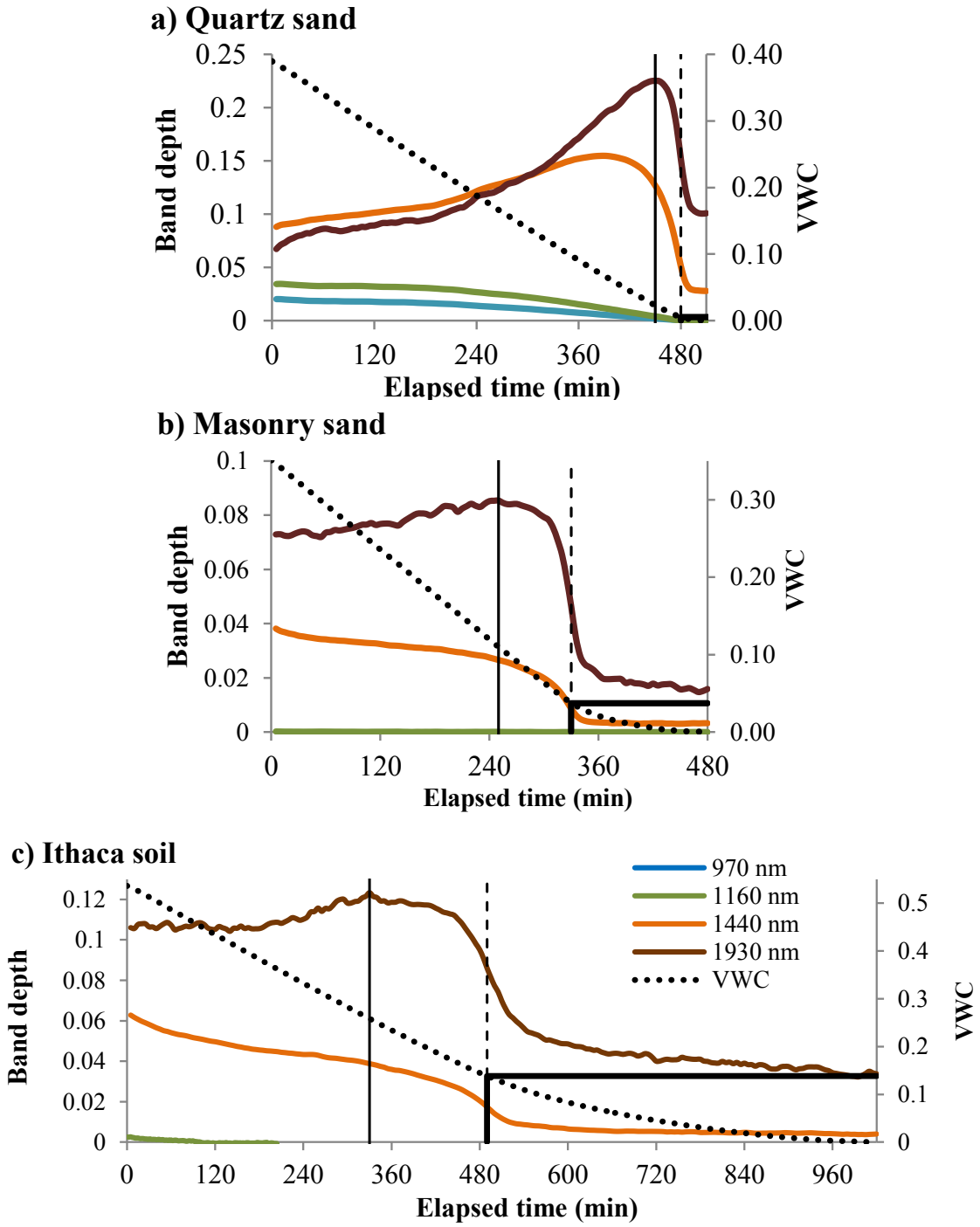

Figure 7: Change in band depth (colored lines) and VWC (dotted black line) with elapsed time from saturation to air-dry; a) quartz sand, b) masonry sand, c) Ithaca soil. The solid vertical line indicates the maximum band depth at the 1930 nm; the dashed vertical lines indicate the minimum (negative) slope at 1930 nm. The heavy black solid lines mark the time and VWC values that coincide with the minimum slope. Figures are scaled to display equal time intervals.

For the longer wavelength absorption bands (1440 nm and 1930 nm) the change in band depth is much more pronounced and clearly nonlinear. Contradicting our initial hypothesis, the band depth is not directly correlated with surface soil water content, nor is it independent of soil type. Instead, the band depth increases with decreasing water content, reaching a maximum near the end of the constant evaporation rate period, then decreasing sharply, finally leveling out and decreasing slowly until the sample is air dry. The explanation for this behavior lies in the contrasting absorption rates between the center and shoulder wavelengths of the absorption band. When the soil is nearly dry, there is very little water in the pore spaces and the band depth is controlled by the very strong absorption ($\sim 137\ cm^{-1}$) at 1930 nm. This is an order of magnitude greater than the absorption at the shoulders of the absorption band (Kou et al., 1993). Thus, for nearly dry conditions, the band depth increases as the water content increases. Once there is sufficient water that there is substantial absorption at the shoulder wavelengths, the 1930 nm light has been almost completely absorbed. From that point until saturation, the change in the band depth is due entirely to absorption at the continuum. Since there is no further absorption at the band center, the band depth decreases as the water content increases. The maximum in the band depth marks the transition between the two absorption rates and is tied to an optical path through the pore water. Fortuitously, this optical path appears to be characteristic of the amount of pore water present at the end of the drying period since the maximum band depth also occurs very near the transition from a nearly constant evaporation rate to a slower evaporation rate. The pattern is illustrated in the following section using a simple model.

2.3.2 A Simple Model

The general pattern of the change in band depth with water content can be duplicated using a very simple model, illustrated in Figure 8. Consider reflectance from a slab of material, covered by a layer of water of depth, h. Radiance, L_d, illuminates the surface, undergoes reflection, R_w, at the water surface, and is refracted into the water at an angle, θ. The radiance propagates through the water, attenuated only by absorption, a. The light is then reflected from a planar surface with reflectance, R_{ws}, which we will assume to be spectrally flat over the range of the absorption band. The reflected light returns to the water surface, again undergoes reflection and refraction, and exits the water surface as radiance, L_u.

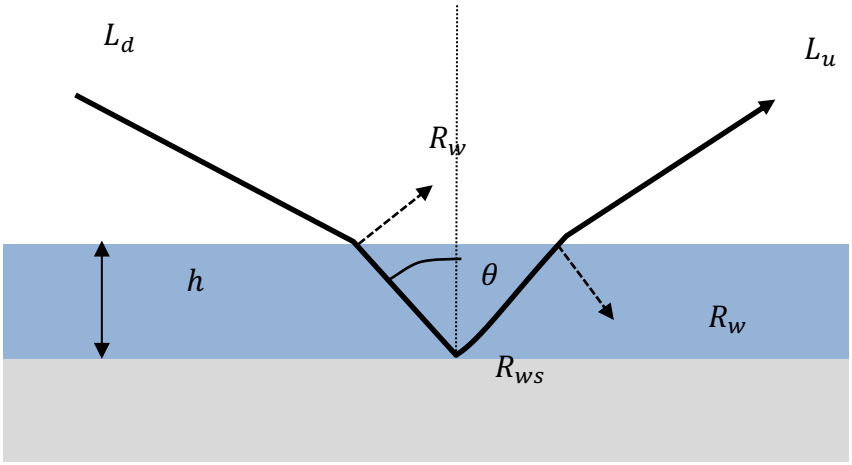

Figure 8: Illustration of a model of reflectance from a spectrally uniform, flat surface covered with a layer of water of depth, h.

The observed radiance, L_u, is given by,

$$L_u = L_d R_{ws}(1 - R_w)^2 e^{-2ah \sec\theta} \quad , \tag{4}$$

which describes the two transmissions at the air-water interface, $(1 - R_w)^2$, a reflection at the water-soil interface, R_{ws}, and the two-way transmission through the water, $e^{-2ah \sec\theta}$. Reflectance is then,

$$R = \frac{L_u}{L_d} = R_{ws}(1 - R_w)^2 e^{-2ah \sec\theta} \quad . \tag{5}$$

Since Fresnel reflectance, R_w, at the water surface is slowly varying spectrally, it is treated as a constant with $R_w \approx 0.02$. For our purposes the angle of incidence will not affect the relative change, and we will consider normal incidence and viewing, $\theta = 0$. Finally, we ignore scattering losses, since over these short distances and at the wavelengths of interest, absorption will dominate the transmission loss. With these simplifying assumptions, the reflectance from the water-coated surface is given by:

$$R = \frac{L_u}{L_d} = k\, e^{-2ah} \quad , \tag{6}$$

where $k = R_{ws}(1 - R_w)^2$. The band depth, ΔR_c, computed with Equation (2) and using Equation (6) to determine the reflectance , can now be written:

$$\Delta R_c = R_{int} - R_c = k[e^{-2a_{int}h} - e^{-2a_c h}] \quad , \tag{7}$$

where $k = 0.96\, R_{ws}$, a_c is the water absorption coefficient at the center of the water absorption band, and a_{int} is the interpolated water absorption coefficient at the band center. The value used for R_{ws} was the reflectance observed from each sample at the point of the minimum slope (dashed line in Figure 7). At that point, the sample appeared dry visually, but the spectrum was noticeably altered indicating that there was water at the surface. The model values for ΔR_c are shown in Figure 9 for the four absorption bands as the depth, h, varies.

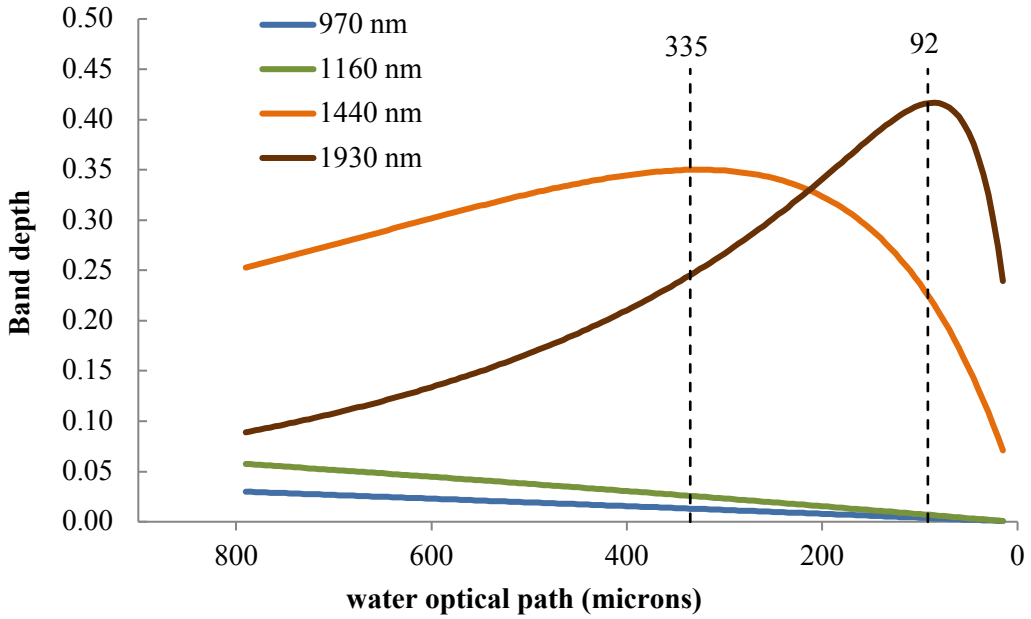

Figure 9: Modeled change in band depth vs. water optical path.

This simple model reproduces the general shape of the curves in Figure 7, most noticeably for the quartz sand. It also provides a basis for considering some of the general properties of the wet soil reflectance. Firstly, all four band depths are described by the same equation in which only the absorption coefficients and the reflectance at the water-soil interface change. The peak observed in the 1930 nm data late in the drying period is a function of the magnitude of the absorption coefficient over the wavelength range and the strength of the contrast between absorption at the center and shoulders of the band. Absorption at the band center, being about an order of magnitude greater than the absorption at the shoulders, dominates the change in band depth for very small h, but after most of the light at the center wavelength has been absorbed, i.e., as $e^{-a_c h} \longrightarrow 0$, further change is controlled by absorption at the shoulder wavelengths.

The depth, h , can be found by taking the derivative of Equation (7), setting it equal to zero and solving for h,

$$h = \frac{ln(a_c/a_{int})}{2(a_c - a_{int})} \quad . \tag{8}$$

For the absorption feature at 1930 nm, the water absorption coefficient at the band center is $a_c = 136.7\ cm^{-1}$, and the interpolated absorption value is $a_{int} = 14.5\ cm^{-1}$, which yields an effective optical depth, $h = 91.8\ microns$. A similar peak is apparent in the band depth curve for 1440 nm. Its location is a function of the absorption coefficients in that wavelength range. The peak is shifted to an earlier time and corresponds to a greater optical path, with $h \approx 335\ microns$. The model predicts a peak for the band depth at 970 nm and 1160 nm band as well, however the absorption coefficients are low enough that light that is not absorbed would be reflected before the required optical path (on the order of a centimeter) is achieved.

This is a simplistic model which serves to demonstrate that there is a link between the observations of the changing band depth at different wavelengths and an effective optical path, h. It has very little applicability beyond this application. An actual optical path in soil is not a depth, as portrayed in the model, but a segmented path that includes multiple reflections and refractions, and represents an average path of all the photons reaching the detector. Another important point is that the model is inappropriate for very small optical paths. In soils, when the water content is very low, the remaining water is usually adsorbed to the particle surfaces, not filling the pore spaces (Nolet et al., 2014).

2.3.3 Sensitivity of the band depth at 1930 nm to VWC

At this point it is worth revisiting the initial hypothesis that the depth of the water absorption bands would be less sensitive to the specific soil type. We consider the absorption band at 1930 nm since it is the most sensitive to change and is strong in all

three samples. In order to remove dependence on drying rate, the band depth is plotted against the volume water content (VWC) in Figure 10. The absorption band depth at 1930 nm is the most sensitive to the volumetric water content (VWC) in general, and is particularly sensitive once the evaporation rate has decreased. The change in band depth with moisture content was far from consistent among the three soil types, i.e., the initial hypothesis clearly fails. Indeed, the magnitude of the maximum band depth varies by almost a factor of three, and the pattern is markedly different for each of the soils. In particular, the maximum band depth occurs at widely different values of VWC. The one consistent characteristic across all three soils is that the band depth increases relatively slowly during most of the drying period, and then decreases rapidly for a relatively short range of VWC.

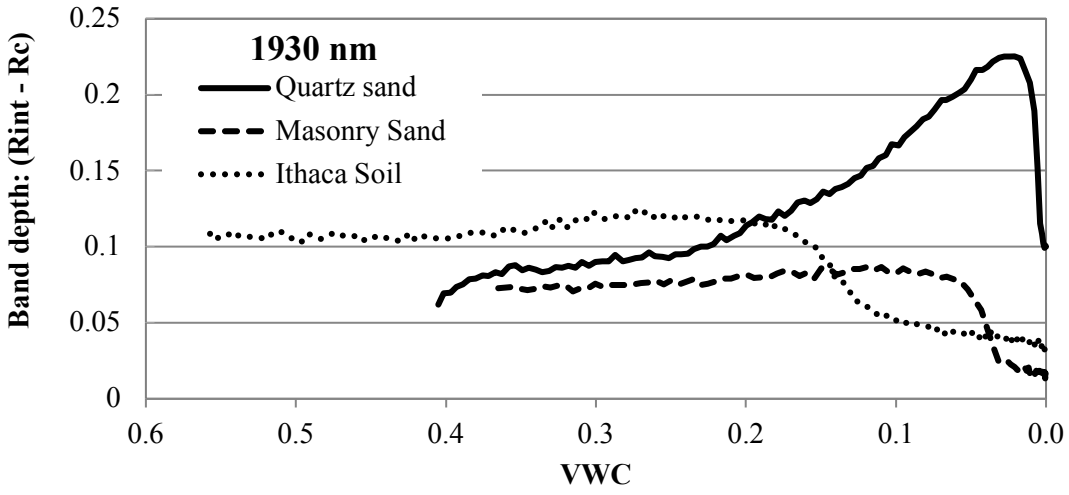

Figure 10: Change in the 1930 nm absorption band depth for the three test soils.

2.3.4 Band depth and VWC

From Figure 7, it is apparent that, although the time required for drying differs substantially and the details of the changes in band depth are quite different for the three soils, the rate of change in VWC is constant for the bulk of the drying period, indicating

a constant evaporation rate. For all three soils, the transition from a constant rate of change in VWC, to a much slower rate at the end of the drying period coincides consistently with the dramatic changes in the band depth at 1930 nm (Figure 7). This is essentially a convenient coincidence. The band depth maximum is associated with a rather specific optical path length, and the rapid decrease in band depth at 1930 nm would correspond to roughly half the optical path length at the maximum. It appears that this range of optical path lengths correlates with the amount of pore water present when the evaporation rate slows from the essentially constant rate when there is more pore water present.

In order to examine this idea further, the drying data are presented again in Figure 11, this time presented together with the evaporation rate, calculated as a 20-minute running average, and plotted against the VWC. The initial evaporation rate was nearly constant, and ranged between 0.0010 and 0.0012 $g \cdot cm^{-2} \cdot min^{-1}$ for all three soils. This initial, steady-state period corresponds to stage-1 drying, a period during which the soil particles are hydraulically connected with a nearly constant water content at the surface, and continuously replenished through a network of water films connecting the pore spaces. Consistent with Figure 7, the vertical lines in Figure 11 represent the maximum band depth (solid line) and the minimum slope (dashed line) for the 1930 nm absorption band. In each case, the band depth features coincide with the transition between stage-1 and stage-2 drying, with the maximum coincident with the beginning of the transition, and the minimum slope occurring once the transition has occurred.

The consistency of the behavior of the 1930 nm band depth and its correspondence to the transition between stage-1 and stage-2 drying is rather surprising given the

differences among the three soil samples. The average particle sizes were very different. The quartz sand consisted predominantly of particles that were 0.05 mm or more in size. The Ithaca soil (silty loam) contained very little sand and much more clay (particle size < 0.002 mm), and shrank significantly during stage-2 drying, leaving a roughly 1 mm space around the edge of the sample holder. The average particle size of the Masonry sand (coarse sand) was intermediate between the other two. In addition, the actual amount of water present in the samples at the time of the transition varied by over an order of magnitude (Table 3). This implies that, regardless of the particle size (or pore size) distribution, the water optical path at the surface prior to the transition from stage-1 and stage-2 drying is enough to remove almost all the light at 1930 nm from the reflected radiation, and that the small amount of water at the surface during stage-2 drying matches the range of effective absorption response at 1930 nm.

Table 3. VWC at transition points for the different soils

	Max. band depth		Minimum Slope	
	Elapsed time	VWC	Elapsed time	VWC
Quartz sand	450 min	0.023	480 min	0.005
Masonry sand	250 min	0.110	330 min	0.037
Ithaca Soil	330 min	0.258	490 min	0.138

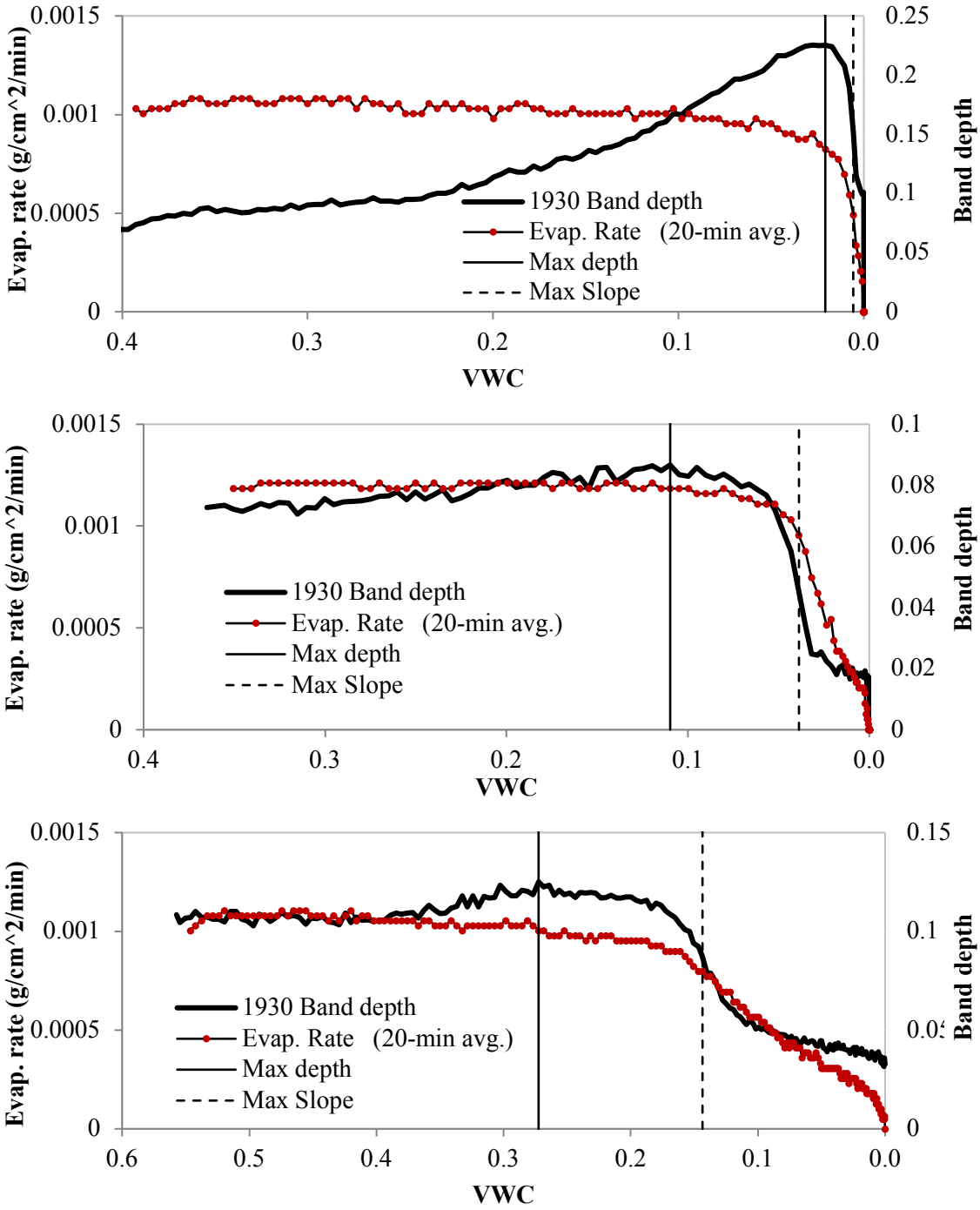

Figure 11: Evaporation rate throughout the drying period for the three soils plotted with the band depth at 1930 nm. The solid vertical line represent the maximum band depth for the 1930 nm absorption band; the dashed line marks the time most rapid change in the band depth for the 1930 nm absorption band.

2.4 Summary and Conclusions

Changes in spectral reflectance with soil water content were examined by monitoring the spectral reflectance and weight of three different soil samples as they underwent evaporative drying, progressing from fully saturated to air dry. The samples were chosen to represent a range of properties: particle size distribution, texture, and drying characteristics, and there were significant differences in the general shape of the spectral reflectance of the three soils when dry.

Working from the assumption that water absorption bands would be the spectral features most sensitive to subtle changes in water content, this paper focused on the most prominent bands in the shortwave infrared, those centered at 970, 1160, 1440, and 1930 nm. Band depth was selected as the primary metric since that would be most likely to be independent of soil type, and would be most directly related to the water content. The band depth for the 970 nm and 1160 nm absorption bands decreased monotonically over time as the VWC decreased. Since the optical path lengths in the soil at these wavelengths were short relative to the attenuation length of water at these wavelengths, the change in band depth was moderate for the quartz sand over the drying time, and was much less – almost undetectable – for the Masonry sand and Ithaca soil (not shown). The change in band depths at the two longer wavelength absorption bands (1440 nm and 1930 nm) was much more dynamic. The 1930 nm band depth was particularly interesting, increasing for much of the drying period as the water content decreased, reaching a maximum near the end of the constant-rate (stage-1) drying period and then decreasing rapidly – a pattern that was consistent for all three soils. As illustrated with a simple model, the band depth maximum resulted from the strong contrast in absorption

coefficients at the center and shoulder wavelengths, with absorption at 1930 nm strong enough that light at that wavelength was almost completely extinguished by absorption after traveling only a short optical path through the soil.

The optical path required to extinguish light at 1930 nm appears to match the very small amount of pore water available near the end of the drying period. As a result, the maximum band depth and the rapid decrease in band depth coincided with the transition from stage-1 to stage-2 drying. This occurred for all three soils even though the particle size (and pore size) distribution, drying time, and water content at the time of the transition varied greatly among the three soil samples.

This was a very limited study, using only three different soil examples. Nonetheless, the results have some interesting consistencies and implications to guide future work:

1. The water absorption bands at 970 nm and 1160 nm have limited capacity for monitoring soil moisture content. The response to water content was only substantial for the quartz sand, which was semi-translucent and had relatively large particle (and pore) sizes. Most agricultural soils are likely to be more similar to the masonry sand or the Ithaca soil, which were opaque and had a wider size distribution, thus limiting the effective optical path of light through the soil.
2. If soil water content is not apparent in the 970 nm and 1160 nm absorption bands, then these bands may be characteristic of the canopy water content only, and not significantly affected by the underlying soil This conclusion presumes that the spectral data have been atmospherically corrected, and supports the estimates of canopy water content derived from these bands (Clevers et al., 2010; Gao, 1996).

3. The water absorption bands at 1440 nm and 1930 nm are extremely sensitive to soil water content over the full range of surface soil water content, from dry to saturated. That the bands are sensitive to water content was expected, but that the sensitivity would span the full range of water content was a bit surprising. It was also surprising that the band depth did not change monotonically with water content, but reached a maximum near the end of the drying period. The band depths at 1440 nm and 1930 nm could be useful in proximal sensing where the user supplies the source light. It will be less useful for remote sensing since absorption by atmospheric water vapor severely depletes the radiation at the center of this wavelength range.
4. The band depth model suggests that it is the contrast in the water absorption coefficients at different wavelengths that is providing the sensitivity to water content. This suggests, in turn, that it is not necessary to observe a full absorption feature, but only enough of the range of the feature to capture a significant attenuation difference. Since atmospheric absorption features are due to water vapor, and are spectrally shifted toward shorter wavelengths relative to liquid water absorption features (Wikipedia, n.d.), it may be possible to make use of the long-wavelength edge of the absorption bands.
5. The maximum band depth at 1930 nm occurs near the end of the stage-1 drying period. There is an order of magnitude difference in the absorption length between the center and shoulder wavelengths. In effect, absorption at the shoulder wavelength is slowly varying while absorption at the center wavelength ranges from minimum (dry) to maximum at characteristic optical depth. Coincidentally, this

optical depth appears to be characteristic of a trace amount of liquid water being present in the pore spaces at the soil surface at the end of the drying period.

It remains to verify and expand on these results by examining a wider range of soil types under controlled conditions, and modeling the underlying processes.

CHAPTER 3: Spectral transmittance of a translucent sand sample with directional illumination

3.1 Introduction

Transmittance of sunlight into soil is a significant issue for both practical problems and theoretical studies. In agricultural applications, the penetration depth of UV, visible and near-infrared (VNIR) radiation into the soil is important for promoting the germination of seeds. Appropriately, transmittance measurements have generally been limited to the VNIR. Particular attention has been given to the 290-500 nm range, which is important for quantification of chemical and biological processes such as photochemical transformation of pesticides or other organic compounds (Balmer et al., 2000; Hebert and Miller, 1990), while 660-730 nm radiation influences seed germination (Benvenuti, 1995; Bliss and Smith, 1985; Woolley and Stoller, 1978).

Transmittance is also related to the depth at which the measured reflectance signal originates – the information depth (Ciani et al., 2005). As such, it is particularly useful in identifying the soil characteristics that contribute to reflectance, and can inform radiative transfer modeling (Banninger et al., 2004; Ciani et al., 2005; Philips-Invernizzi et al., 2001). Fenchel and Staarup (1971) found that the penetration depth was very sensitive to the particle size distribution, and was rather strongly wavelength dependent in rinsed quartz sand. Woolley and Stoller (1978) found very strong wavelength dependence in the transmittance of a sand sample relative to that of a silty clay loam. Other studies have shown that penetration is deeper at longer wavelengths, and that particle size distribution influences the light penetration (Bliss and Smith, 1985; Haardt

and Nielsen, 1980). Explicitly, Bliss and Smith (1985) found that transmittance decreased sharply as the size of the sand particles decreased. Neema et al. (1987) reported and modeled data from Shah (1981) indicating that transmittance of visible light initially increased with moisture content, but then decreased as the pore spaces filled, a finding not noted elsewhere. Recent work has focused on the directional character of reflectance, i.e., the Bidirectional Reflectance Distribution Function (BRDF) (Bachmann et al., 2014; Baranoski et al., 2014). Given the sensitivity of the BRDF to the structure of the soil (e.g., density, pore space, particle size), this work suggests that there would also be a directional character to the transmitted radiation.

In this paper, the purpose of viewing the change in transmission with illumination angle is to gauge the significance of forward scattering within the soil, and to consider how a change in illumination angle might affect the penetration depth. The authors' previous studies (Tian and Philpot, 2014, 2016, 2015) showed that soil moisture strongly influences reflectance, but the relative importance of absorption and scattering remained unclear. The transmittance experiments presented here are intended to supplement the reflectance study, and help to separate the effects of internal scattering and absorption. The eventual goal is to have a general model that will characterize wet soils.

Models of scattering by single particles that are large relative to the wavelength of incident light indicate that forward scattering will be strong, due in part to diffraction and reflection, and in part to refraction of transmitted light (Kimmel and Baranoski, 2007; Hapke, 2012). While diffraction effects can generally be ignored for ensembles of particles (Hapke, 2012), the transmission and multiple scattering effects remain,

raising the possibility of a distinctly directional scattering phase function near the surface. While there are a number of examples of measurements of directional reflectance/scattering from soil surfaces (Bachmann et al., 2014; Deering et al., 1990; Souchon et al., 2011), the authors are not aware of any observations related to directional forward scattering in a medium as complex as soil. However, computational examples and observations exist for scattering by clusters of particles (Comberg and Wriedt, 1999; Holler et al., 2000, 1999; Videen et al., 1999). These suggest that the forward scattering will be both complex and sensitive to the size distribution, spacing and organization of the cluster, and would have implications for the effectiveness of attempts to invert the observations to extract information about the structure of the soil.

In this paper, we measure the spectral transmittance of sand samples under both dry and saturated conditions, primarily focusing on how sand transmittance changes with varying illumination angle, and how adding water influences sand transmittance. We extend the sand layer transmittance measurements from the visible through the SWIR. Mandoli et al. (1990) indicated that sand transmittance increased dramatically with added water over 400-800 nm, however, transmittance should decrease in SWIR region due to the strong water absorption at longer wavelengths. Though the added water decreases the relative index of refraction at the surface of the sand particle, which is the reason for transmittance increase at shorter wavelengths (Hoa, 1981), water absorption is dominant at longer wavelengths, especially in the strong water absorption bands. Our initial hypothesis was that strong forward scattering characteristic of single particles and clusters of particles would be apparent in dense sand samples, and that this would be observable as a rapid decrease in transmittance as the angle of illumination increased.

While forward multiple scattering would be less distinct than single scattering, we expected the prominent forward scattering to be apparent in the transmittance measurements. Furthermore, while a wet sample might have an enhanced forward scattering in the VNIR region, the transmittance should fade quickly at longer wavelengths.

3.2 Experimental design

The work described here was designed to observe the change in penetration of light through a shallow sand sample as the incidence angle of the light source was varied from 0-70° under both air-dry and saturated conditions. In order to observe the influence of varying sand properties, five samples using two different materials with varied characteristics were monitored. Since transmittance was difficult to observe with dark samples due to the strong absorption, our observations were necessarily restricted to materials with low absorption. In this experiment, a translucent quartz sand sample, and an opaque, white aluminum oxide sand were observed. All experiments considered light over the spectral range 350-2500 nm.

3.2.1 Sand sample

The first three samples consisted of the same white, translucent quartz sand, and the last two samples consisted of pure aluminum oxide particles. As shown in Table 4 and Figure 12, samples 1 and 2 were quartz samples that differed in bulk density but had the same depth, while samples 1 and 3, both quartz sand with the same bulk density, demonstrate the influence of sample depth on the observations. The quartz sand sample, acquired from a golf course in Ithaca, NY, consisted of rough, quartz particles, and had a slightly yellowish color (Tian and Philpot, 2015). The experiment was repeated using

samples 4 and 5, a white aluminum oxide with a uniform particle size, purchased from Kramer Industries (Kramer Industries, n.d.). The experiment examined two different bulk densities. To estimate the porosity of the five samples, the material density of Samples 1 to 3 was estimated as 2.65 g/cm^3, which is the quartz material density, and also the most commonly used density for sand particles (NRCS, n.d.). Sample 4 & 5 were pure, white aluminum oxide with a material density of 3.95 g/cm^3. Water was added slowly at the sample surface from one edge of sample holder, taking care not to disturb the sample surface near the detector field of view. Water was added until the sand surface was uniformly dark, i.e., the sample was near saturation internally, with a surface water film on the particles, but without water filling the surface pore spaces and no free liquid water at the surface. Therefore, the volumetric water content (VWC) was not consistent with the estimated porosity in Table 4. Below the surface, the sample was internally saturated.

Table 4. Sample properties

	Sample 1	Sample 2	Sample 3	Sample 4	Sample 5
Material	Major SiO_2	Major SiO_2	Major SiO_2	Pure Al_2O_3	Pure Al_2O_3
Texture	Coarse sand				
Particle size (mm)	1.1% 1.0-2.0 mm; 85.0% 0.5-1.0 mm; 10.1% 0.25-0.5 mm; 3.6% 0.1-0.25 mm; 0.2% 0.05-0.1 mm; 0% silt or clay.			0.425	0.425
Depth (mm)	3	3	4	3	3
Bulk density (g/cm3)	1.19	1.32	1.19	1.65	1.97
Estimated porosity	0.55	0.50	0.55	0.58	0.50
VWC when wet	0.39	0.42	0.39	0.58	0.50

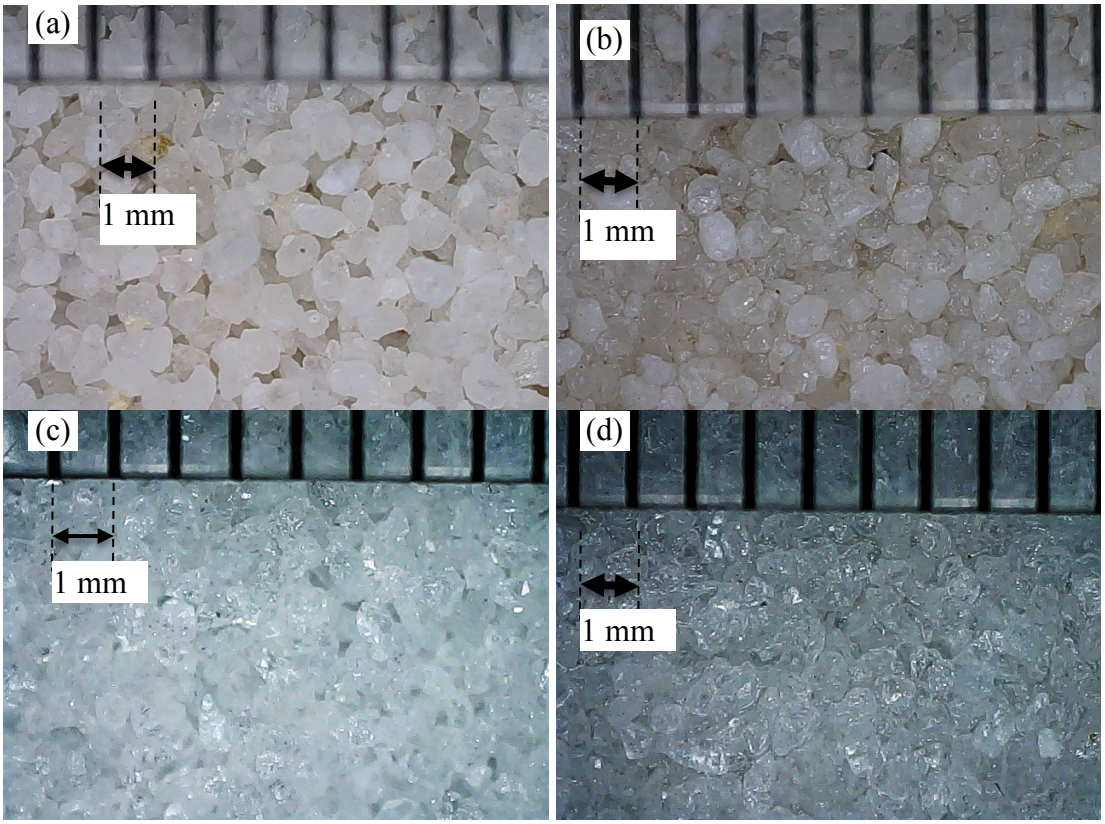

Figure 12. Microscopic images of the sand samples: quartz sand: (a) air-dry, (b) saturated; aluminum oxide: (c) air-dry, (d) saturated.

3.2.2 Experimental setup

Figure 13 shows a sketch and a photo of experimental apparatus. Illumination was provided by an ASD Pro Lamp, a 50 Watt halogen-based light source designed to provide stable illumination over the 350 to 2500 nm range. The lamp was mounted on a 1.12 m-long arm (r_0), which was attached to an RM-5 motorized rotary stage from Newmark systems Inc. The rotary stage was mounted vertically on the base frame, allowing automated positioning of the light source at specific illumination angles. The spectrometer, an ASD FieldSpec® 4, has a spectral range of 350–2500 nm. The spectral resolution of the spectrometer ranges from 3 nm in the visible to 12 nm at 2100 nm, with a sampling interval of 1 nm. A fiber optic probe, fitted with a 3° field of view (FOV) fore optic, was placed below sample holder pointing directly upward and was directly in line with the light source when lamp was in the zenith position.

The sample holder, illustrated in Figure 14, consisted of a cylindrical base with an internal ledge designed to hold a 10 cm diameter, 6.5 mm thick, uncoated, BOROFLOAT® Window (Edmund Scientific, 2016), with better than 90% transmittance over the 350-2000 nm range. Transmittance of the window degrades beyond 2000 nm, but remains above 70% at 2500 nm. The edge of the sample holder base was flush with the top surface of the optical window. Rim inserts, designed to fit into a ridge on the outer edge of the base, define the sample depth. For the control measurement and bulk density-variable experimental measurement reported here, a 3 mm deep rim insert was used (Figure 14). For the sample depth-variable experimental measurement, both 3 mm and 4 mm deep rim inserts were used. In each case, the sample surface was positioned at the axis of motorized rotary stage. In order to minimize

reflections from below, the support for the sample holder was lined with black felt except for a viewing port for the fore optic. In the experiments, the sample holder was initially filled with a dry sample, and the surface was leveled with a metal straight edge providing a uniform, level surface. Figure 3b shows the plan view of the sample holder shown in the experimental apparatus Figure 13. To present clearly, only half sand sample was added; the 3° fore optic can be seen on left side with white paper as background for better contrast. In experiment, the fore optic was viewing the center of the sample holder and the sand was distributed evenly.

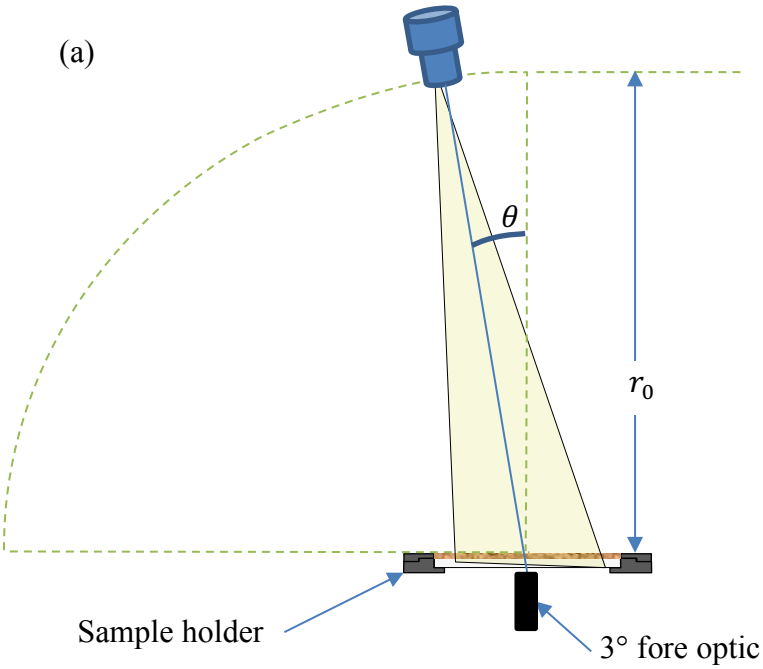

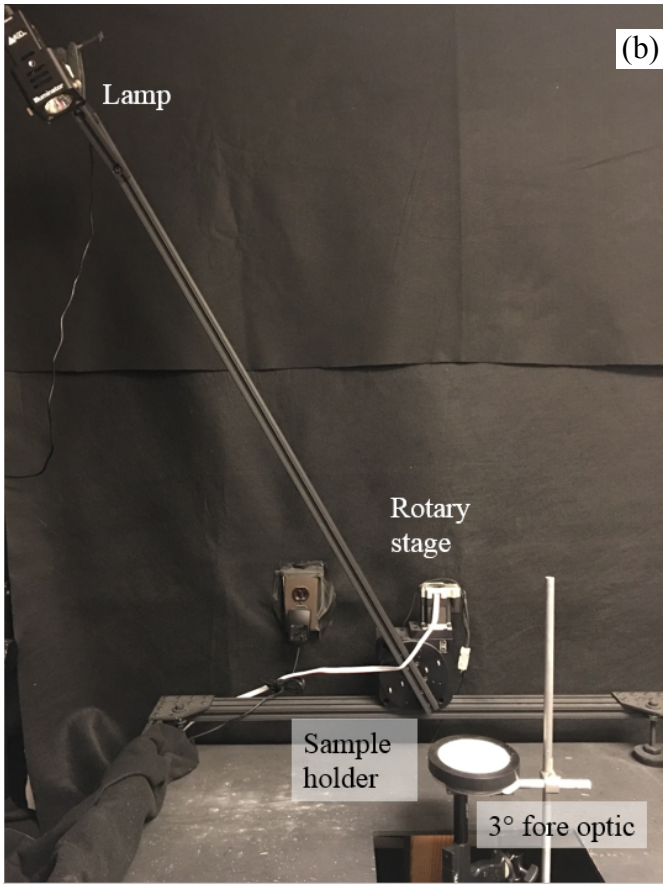

Figure 13. Experimental apparatus: (a) sketch, (b) photo.

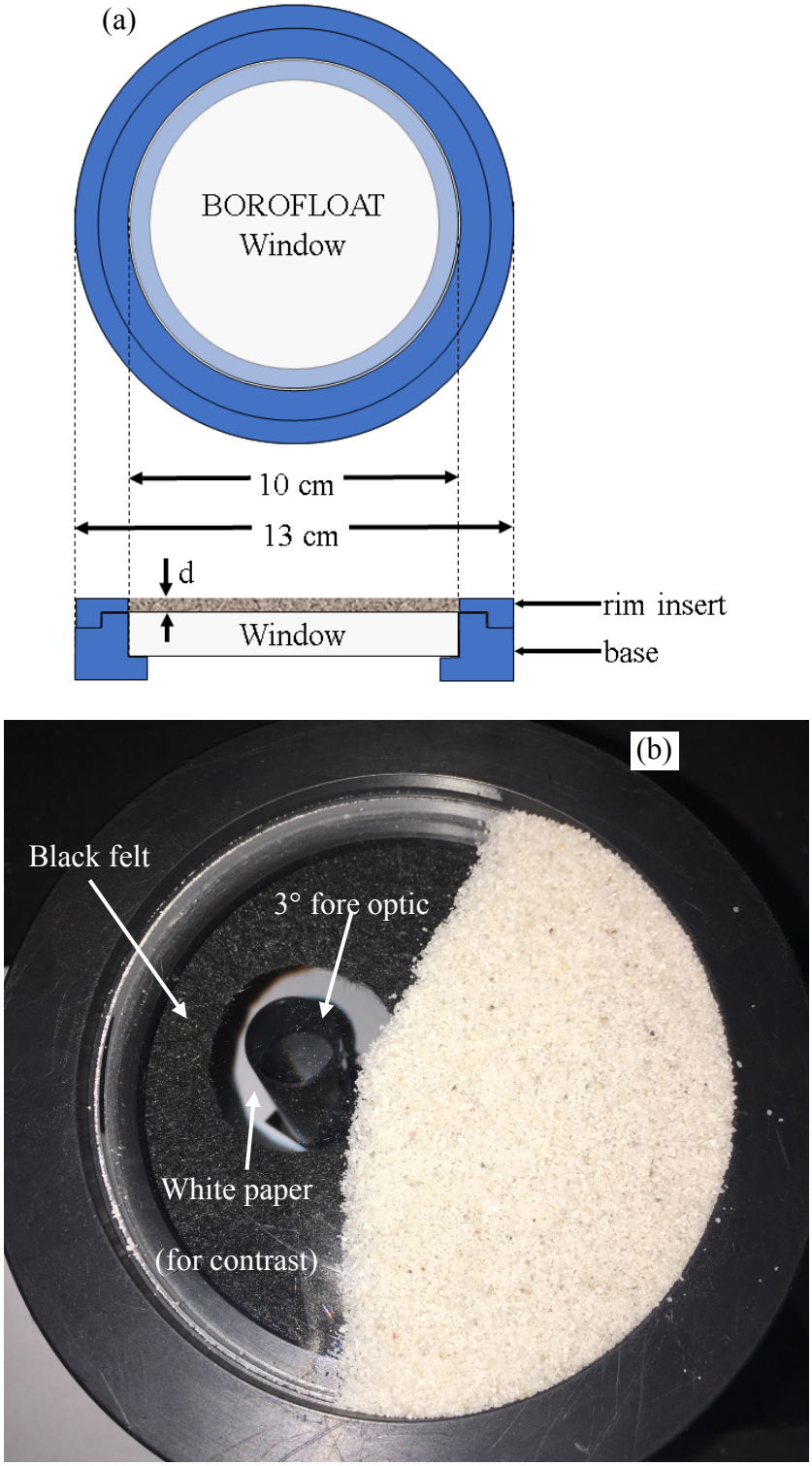

Figure 14. Sample holder: (a) design sketch and (b) photo (with half sample).

3.3 Experimental procedure

To calculate transmittance through sample, the radiance at the sample surface and the transmitted radiance through sample are necessary. The transmittance of the window must also be considered.

3.3.1 Irradiance at the sample surface

Since the FieldSpec®4 spectrometer saturated – even at the shortest integration time – when viewing the light source directly, an alternate procedure was required to determine the radiance at the sample surface. This was done by observing the reflectance of a calibrated, diffuse reflectance standard and computing the radiance at the surface. The experimental setup is the same as that shown in Figure 15 but without the BOROFLOAT window.

A 99% reflectance, calibrated Spectralon® panel was illuminated from the zenith direction, and the radiance was observed at a small angle. The assumption was that the reflectance panel was very nearly Lambertian at small angles. An observation angle of 5 degrees, represented as θ_{std} in Figure 15, was sufficient to avoid any shadowing of the sample by the 3° fore optic. With the measured radiance at 5° represented as L_{std}, the irradiance at the sample surface, E_0, is calculated as:

$$E_0 = \frac{\pi \cdot L_{std}}{R_{std} \cdot cos\,(\theta_{std})} \quad , \tag{9}$$

where R_{std} is the calibrated reflectance of the Spectralon® standard.

3.3.2 Transmittance of the BOROFLOAT® window

To characterize the BOROFLOAT® glass transmittance, the window was placed on top of the reflectance standard for radiance measurements as shown in Figure 15.

Radiance transmitted through the glass window is reflected by the standard and detected at θ_{std}. The radiance, L_g, observed at the detector is then given by:

$$L_g = \tau_0 \tau_{\theta_{std}} \left(1 - R_{ag}\right)^4 E_0 \cos\theta_{std} R_{std}/\pi \quad , \tag{10}$$

where R_{std} is the reflectance of a Lambertian standard, $\tau_{\theta_{std}} = \exp\left(-a_g d_g \sec\theta_{std}\right)$ is the transmittance of the incident radiation, τ_0 is the transmittance of the reflected radiation vertically through the glass ($\tau_0 = \tau_{\theta_{std}}$when $\theta_{std} = 0$), a_g is the absorption coefficient of the glass window, d_g is the thickness of the window, and R_{ag} is the Fresnel reflectance coefficient for normally incident light at the air-glass interface. With $\theta_{std} = 5°$, and $\sec\theta_{std} = 0.996$, the effective transmittance, τ_g, of the glass window can be approximated as:

$$\tau_g \cong \sqrt{\tau_0 \tau_{\theta_{std}}}\left(1 - R_{ag}\right)^2 = \sqrt{L_g/L_{std}} \tag{11}$$

where L_{std} represents the radiance collected from the reflectance standard directly (without the glass window), and L_g is the radiance collected (Figure 15). The reflectance at the air-glass interface is included in the transmittance factor since the surface loss is a consistent contribution to the transmittance factor.

Figure 16 shows the experimentally determined spectral transmittance of the glass window. As mentioned above, the transmittance is high from 350 nm to 2000 nm, above 96% except for an absorption feature centered at 1400 nm. At wavelengths greater than 2000 nm, transmittance decreased.

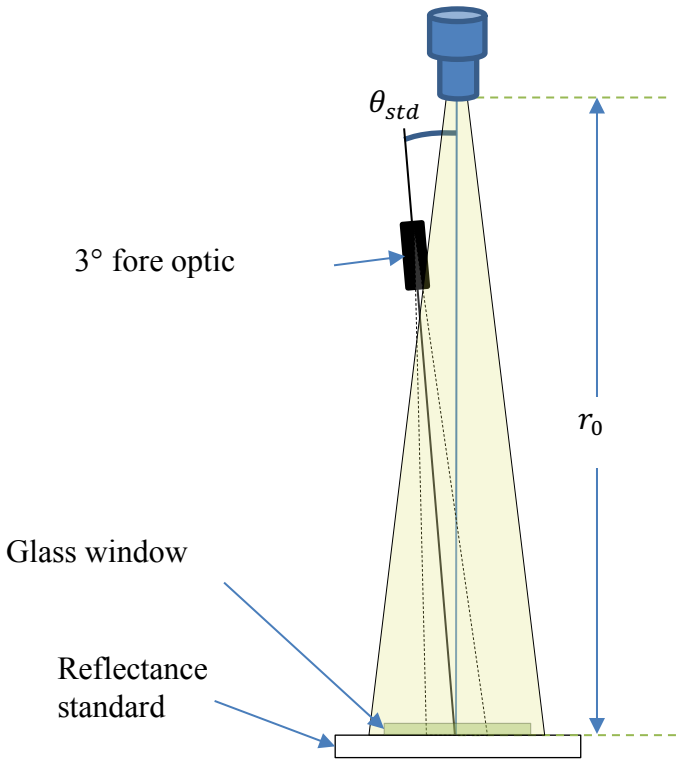

Figure 15. Glass window transmittance estimate setup.

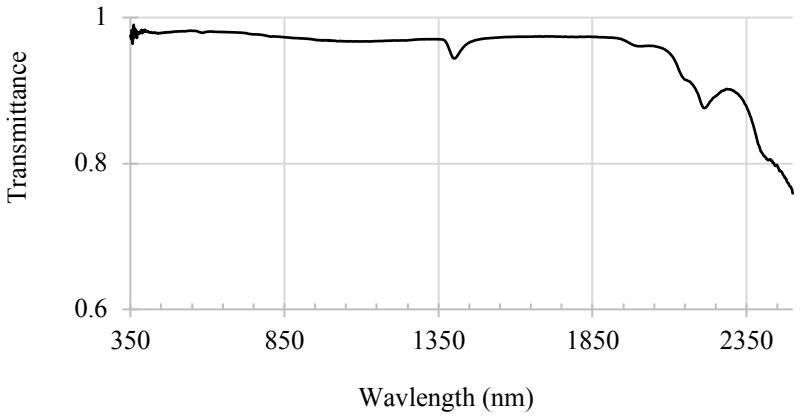

Figure 16. Glass window transmittance estimate.

3.3.3 Transmitted radiance measurements

Transmitted radiance measurements were made using the arrangement illustrated in Figure 13, with the fore optic viewing vertically upward through the quartz glass window and sand sample. The lamp, controlled by the RM-5 motorized rotary stage, was positioned at 5-degree intervals from 0-70°, at a fixed distance, r_0, from the sample surface. Observations were restricted to the left side because the support for sample holder would have blocked light from right. The integration time was set with the lamp in the 0° position, and the same integration time was used for all illumination angles.

3.3.4 Transmittance calculation and experimental procedure

The light source was far enough away from the sample holder that the area covered by the lamp beam was significantly larger than field of view of the detector, and much larger than the depth of the sample. After reflective loss, $1 - R_\theta$, at the surface, the irradiance propagates diffusely through the sand sample, attenuated by scattering and absorption:

$$E(z, \theta) = (1 - R_\theta) \cdot E_0 \cos\theta \cdot e^{-kz} \quad , \tag{12}$$

where the attenuation coefficient, k, accounts for both scattering and absorption losses, and z is the average optical depth. Note that, due to multiple scattering, the average optical path through the sample is proportional to but greater than the sample depth. We also assume that the sand sample is optically uniform (i.e., a uniform particle size distribution and uniform orientation) both horizontally and vertically, so that k may be taken as a constant for a given wavelength. Transmittance may then be defined as

$$T = \frac{E(z,\theta)}{E(0,\theta)} = e^{-kz} \quad . \tag{13}$$

After passing through the quartz window with transmittance, τ_g, there is reflective loss at the glass surface, R_{sg} (a combination solids/glass and air/glass interface when dry, or water/glass when saturated), the irradiance at the detector is

$$E_{det}(z,\theta) = (1 - R_{sg})\tau_g E(z,\theta) \quad . \tag{14}$$

Assuming that the irradiance at the detector is essentially diffuse, the observed radiance is simply

$$L_{det}(z,\theta) = \frac{E_{det}(z,\theta)}{\pi} \quad . \tag{15}$$

An expression for the transmittance of a sample may now be written in terms of the observed radiance by combining Equations (5), (6) and (7):

$$T = \frac{\pi \cdot L_{det}(z,\theta)}{\tau_g \cdot (1 - R_\theta)(1 - R_{sg}) \cdot E_0 \cdot cos\,\theta} = e^{-kz} \quad , \tag{16}$$

where $L_{det}(\theta_{src})$ is the radiance at the detector below the sand sample, and R_θ is the reflective loss at the sample surface. Substituting for E_0 using Equation (1), we may write:

$$T = \frac{L_{det}(z,\theta)}{\tau_g \cdot cos\,\theta} \cdot \frac{cos(\theta_{std})\,R_{std}}{(1 - R_\theta)(1 - R_{sg}) \cdot L_{std}} = e^{-kz} \,. \tag{17}$$

Since R_θ and R_{sg} are unknown, our transmittance measurements are computed as:

$$T' = \frac{L_{det}(z,\theta)}{\tau_g \cdot cos\,\theta} \cdot \frac{cos(\theta_{std})\,R_{std}}{L_{std}} = (1 - R_\theta)(1 - R_{sg}) \cdot e^{-kz} \,. \tag{18}$$

All quantities in the center expression of Equation (18) are known. Measurements were first made with air-dried samples. The samples were then saturated with water and

the sequence was repeated. Water was added at the edge of the sample holder farthest from the viewing port in order to minimize changes of particle distribution within the viewing area.

3.4 Results

3.4.1 Dry sample transmittance

Transmittance spectra for the three quartz samples under dry conditions are shown in Figure 17a, b, and c. The shapes of the transmittance spectra are similar for all three dry samples. Excepting the anomalously high transmittance in Figure 17a with $\theta = 0°$, when the detector is directly in line with the lamp, the magnitude decreases gradually and uniformly as the illumination angle increases. The dry, low bulk density sample 1 (Figure 17a) has the greatest average transmittance among the three quartz samples. Interestingly, the transmittance spectra of samples 2 & 3 (Figure 17b, c) are very similar in magnitude, with that for sample 3 – the deeper, low density sample – being only slightly lower.

Figure 18a, b show the transmittance of the dry Aluminum Oxide sample, samples 4 & 5, at varying illumination angles. The transmittance of the dry, high bulk density sample is generally lower than that of the dry, low bulk density sample, which is consistent the quartz sand sample results. This is as expected, since the higher density should increase the probability of scattering and absorption. (The small impulse at 694 nm is caused by Cr^{3+} impurities in the Al_2O_3.) Compared to Figure 17, the transmittance of Al_2O_3 is relatively high in the visible, and is more uniform over the spectrum. The gradual decrease in transmittance with changing illumination angle for Al_2O_3 is similar to that for quartz sand. As with the quartz sand, transmittance through the Al_2O_3 at the

0° illumination angle is slightly stronger than might be expected from the change with angle (Figure 18a), but only slightly.

3.4.2 Saturated sample transmittance

For the saturated samples (Figure 17d, e, f, and Figure 7c, d) there are three general differences relative to dry samples: 1) water absorption features dominate at longer wavelengths, 2) transmittance is enhanced in the VNIR region, 3) transmittance changes with increasing illumination angle occur at about the same rate for both dry and saturated samples. One particular difference between dry and wet low density samples (Figure 17a, b and Figure 18a, b) is that, the anomalously high transmittance at $\theta = 0$ only occurs with the dry samples; it is not apparent in the wet sample spectra.

3.4.3 Transmittance change with illumination angle

Our observations did not support the presence of strong, forward scattering from the directional illumination, nor did they provide any evidence of a complex structure in the transmitted light. As seen in Figure 16 and Figure 17, the change in transmittance is gradual and directly proportional to the incidence angle. Exceptionally high transmittance only occurs with the dry, low-density, 3-mm deep samples, and only at the 0° scattering angle. There is no apparent increase at 5 degrees. Even this small, 0° anomaly disappears with higher bulk density at the 3-mm depth (Figure 17b and Figure 18b) or at the low density and a greater depth increment (Figure 17c). While it is possible that the scattering pattern is more complex at shallower depths, at the shallowest depth at which it was feasible to make these observations, the transmitted radiation is already effectively diffuse.

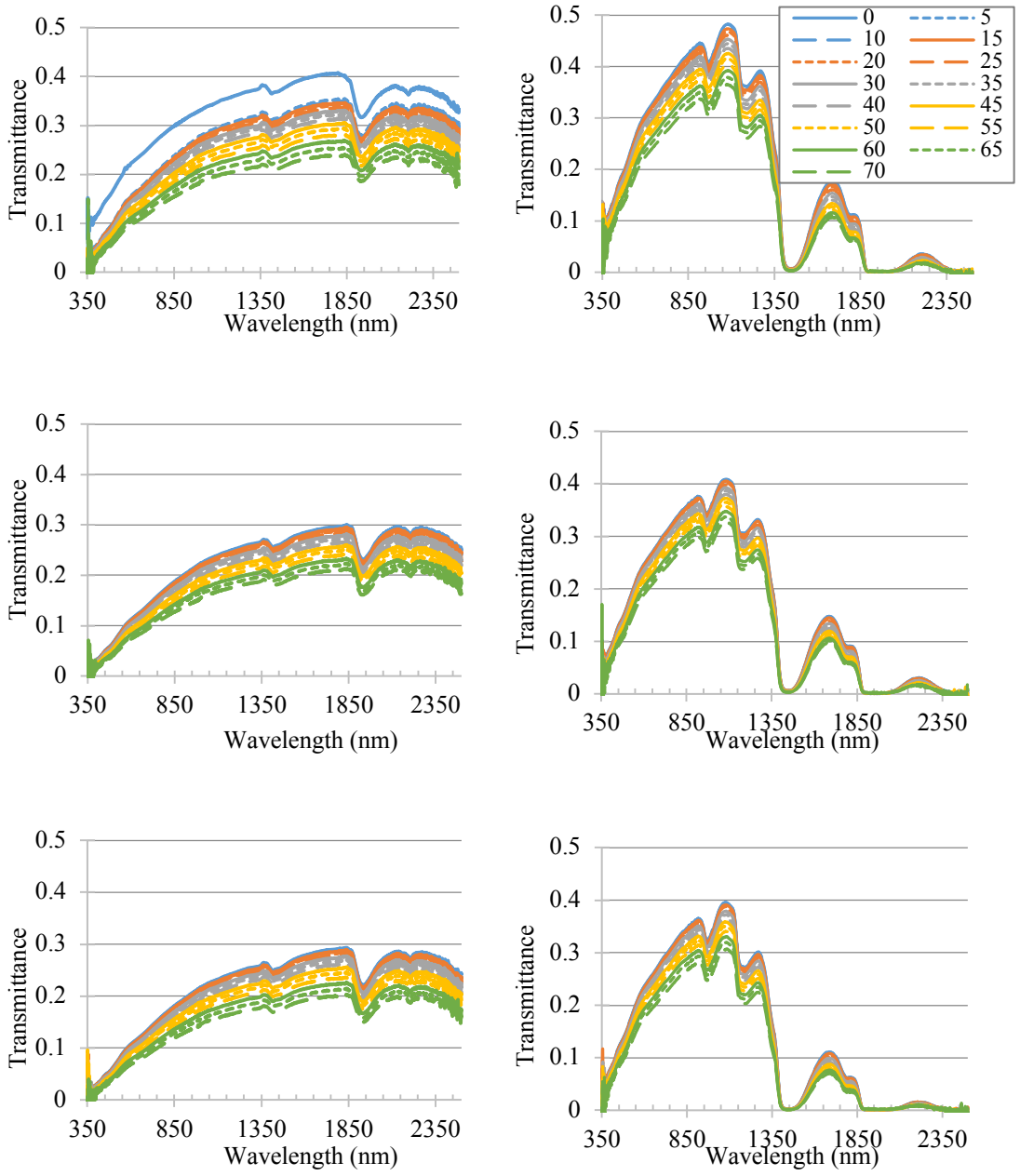

Figure 17. Transmittance for the quartz sand samples 1, 2 and 3 under air-dry (a, b, c) and saturated (d, e, f) conditions, respectively, with the illumination angle changing in 5° increments from 0-70°.

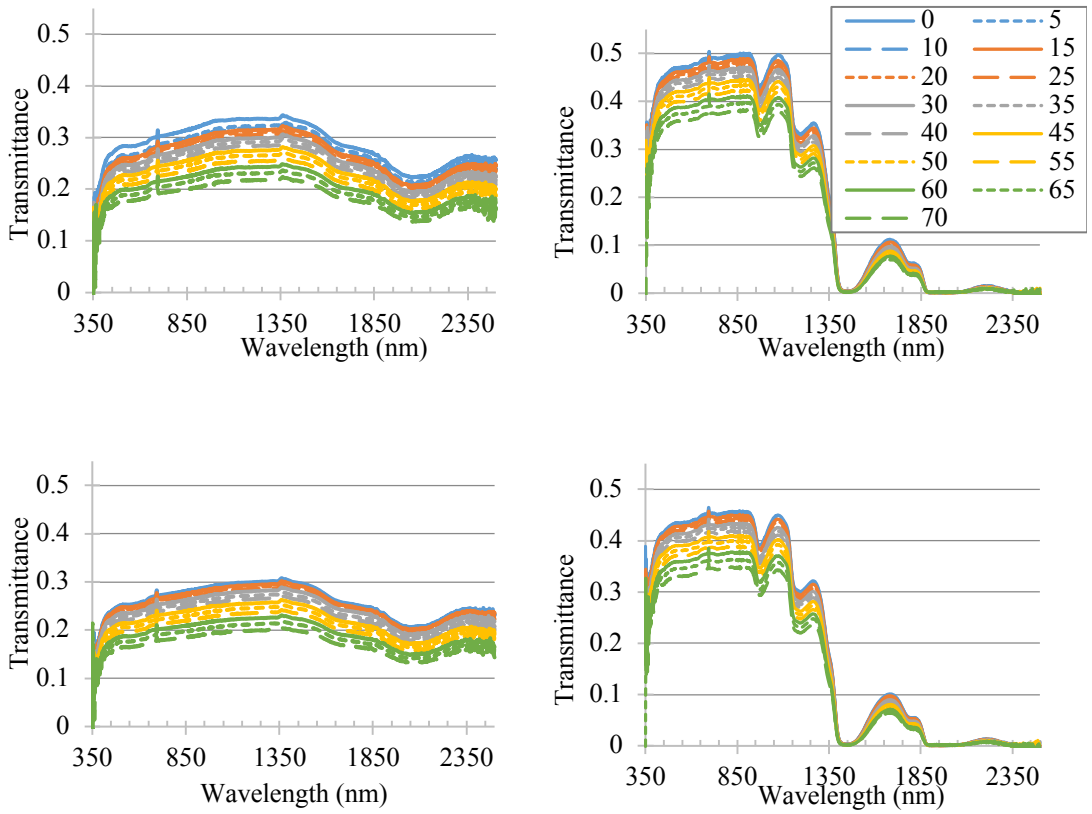

Figure 18. Transmittance for the Al_2O_3 samples 4 and 5 under air-dry (a, b) and saturated (c, d) conditions, respectively, with the illumination angle ranging from 0-70°, in 5° increments.

3.4.4 Water influence on spectral transmittance

In the SWIR region, water absorption dominates as seen in Figure 17d-f and Figure 18c-d. This is especially true at the two strong water absorption bands, centered at 1440 nm and 1930 nm, where water absorption is so strong that radiation scarcely reaches the detector. At 1700 nm, between the strong water absorption bands, transmittance is substantially reduced, confirming the dominance of water absorption at the longer wavelengths.

The striking contrast between the VNIR and SWIR transmittance of the saturated samples can be explained by the range of the water absorption coefficient – 6 orders of

magnitude – between 400 nm and 2500 nm (Kou et al., 1993; Pope and Fry, 1997). The high water absorption coefficient in the SWIR region insures that light is absorbed over very short path lengths. As can be seen in the spectra of all five samples, an important transition occurs near 1300-1330 nm. Table 5 lists the wavelength at which the transmittance of the wet sample changes from greater than, to less than that of the dry sample based on the spectrum for the 5° illumination angle. The water absorption coefficient ranges from 1.3 – 2.2 cm^{-1} in the 1300 to 1330 nm interval. In effect, at wavelengths less than 1300 nm absorption is primarily due to the sand particles; at wavelengths greater than 1330 nm, when water absorption coefficient is larger than 3.1 cm^{-1}, water absorption is the dominant feature.

Table 5. Boundary wavelength to distinguish forward scattering and water absorption domination

Sample 1	Sample 2	Sample 3	Sample 4	Sample 5
1322 nm	1324 nm	1312 nm	1319 nm	1307 nm

In Figure 19, three wavelengths representing the visible (500 nm), NIR (900 nm), and SWIR (1700 nm) are selected to illustrate the change in transmittance with illumination angle and to compare the water influence on sand transmittance. In addition, a band representing a weak water absorption feature in the NIR (970 nm) is illustrated. As was seen in Figure 17a, the transmittance of the low-density quartz (Sample 1) is more pronounced with illumination at zenith than it is at tilted angles. Except for zenith illumination, transmittance decreases gradually with increasing illumination angle. Transmittance increases in the VNIR when the sample is wet. This is a direct consequence of the reduction in the relative index of refraction when the water/particle

interface replaces the air/water interface (Twomey et al., 1986). The increase in forward scattering is large enough that, the transmittance of the saturated sample is stronger than that of the dry sample. This is true even at center of the water absorption feature at 970 nm. At the SWIR wavelength (1700 nm), the effect of adding water is to drastically reduce transmittance due to absorption by the water. As with the dry sample, transmittance decreases gradually with increasing illumination angle.

The general pattern is repeated for the low-density Al_2O_3 (Sample 4, Figure 18b). In this case the dry reflectance is nearly the same for all the selected wavelengths, and the rate of decrease in reflectance with illumination direction is also very similar. There is only a slight increase in transmittance at normal incidence. As with the quartz, transmittance increases markedly in the VNIR channels when the sample is saturated, and decreases sharply in the SWIR channel. There is also difference in the pattern of decreasing transmittance with the dry sample curves being slightly convex, and the wet sample curves being slightly concave.

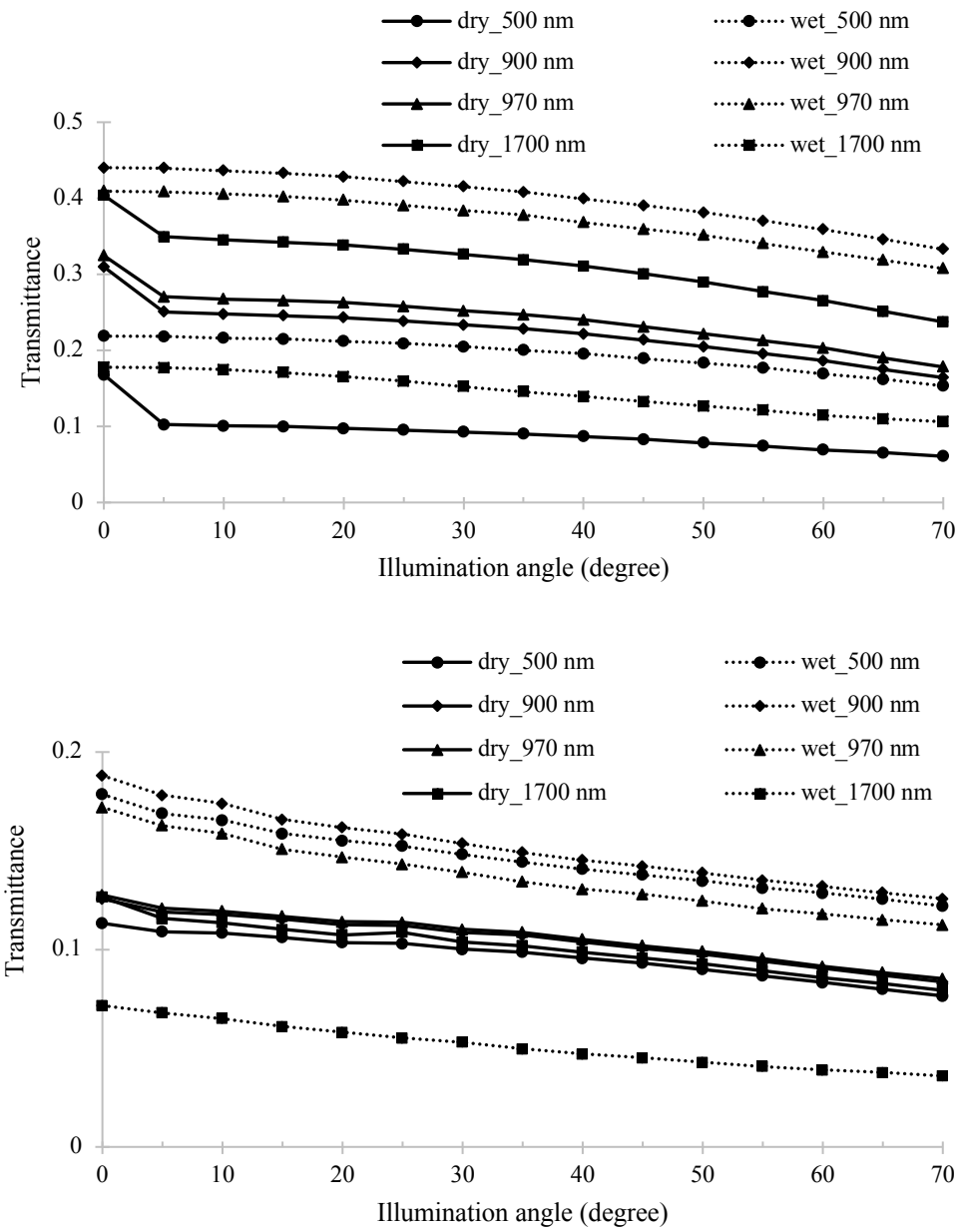

Figure 19. Transmittance comparison for a) low-density quartz (Sample 1), and b) low-density Al_2O_3 (Sample 4) between dry and saturated conditions at 500 nm, 900 nm, 970 nm and 1700 nm.

3.4.5 Angular dependence of transmittance

To study how different components influence transmittance with varying illumination angle, Equation (10) is recalled. Because the average optical depth, z, should be related to illumination angle, it is represented as $df(\theta)$, where d is the sample depth, and $f(\theta)$ represents the weighted value. Then, Equation (18) can be rewritten as:

$$T' = (1 - R_\theta)(1 - R_{sg})e^{-kdf(\theta)} \quad . \tag{19}$$

To study the relationship between transmittance, T', and sand thickness, d, the natural logarithm is taken of Equation (19), yielding,

$$ln\, T' = ln(1 - R_\theta)(1 - R_{sg}) - kdf(\theta) \tag{20}$$

Given the apparent diffuse nature of the radiation, it is reasonable to assume that the 3 mm low density and 4 mm low density quartz sand samples would have the same extinction coefficient, k, since the sample composition and bulk density are constant. To examine this assumption, kf(θ) is calculated by taking the derivative of Equation (20) with respect to depth. The results are plotted in Figure 20 vs. illumination angle in both dry and wet conditions. Figure 20 suggests that $kf(\theta)$ is not sensitive to the illumination angle; indeed, the illumination angle appears to have no influence on attenuation within a sand sample.

A second point worth noting in Figure 20 is that $kf(\theta)$ decreases in the VNIR when wet, and increases in the SWIR. Since there is no angular dependence, $f(\theta)$ is expected to be the same whether the sample is dry or wet. The corollary is that these differences are due entirely to the extinction coefficient. The decrease in attenuation in the VNIR is consistent with the increase in forward scattering (and decrease in backscattering) due

to the change in the relative index of refraction. The increase in attenuation in the SWIR is consistent with the increase in absorption by water. The lack of angular response is consistent with the assumption that the forward scattered light is diffuse and not directional.

If attenuation is independent of the illumination angle, then sensitivity to illumination must be due to reflectance. The intercept, $ln(1-R_\theta)(1-R_{sg})$ can be determined by linear fitting of equation (20) using the two samples at different depths. The resulting values of $(1-R_\theta)(1-R_{sg})$ in Figure 21 show a clear, almost linear sensitivity to illumination angle in both dry and wet conditions. At all four wavelengths, $(1-R_\theta)(1-R_{sg})$ is always higher when wet; the increment is ~20%. This is due to the smaller relative refractive index of water/particle compared to air/particle. The average $(1-R_\theta)(1-R_{sg})$ is always lower for the wet sample (i.e., wet soil is darker than dry soil).

Since the refractive indices (real part) of air, water and quartz (silicon) are only weakly sensitive to wavelength over 350-2500 nm (Hale and Querry, 1973; Kitamura et al., 2007; Kou et al., 1993), it is reasonable to assume that R_{sg} is constant with respect to the illumination angles under either dry or wet condition. Then, the linear sensitivity to illumination angle shown in Figure 21 should be primarily related to the surface reflective loss, R_θ.

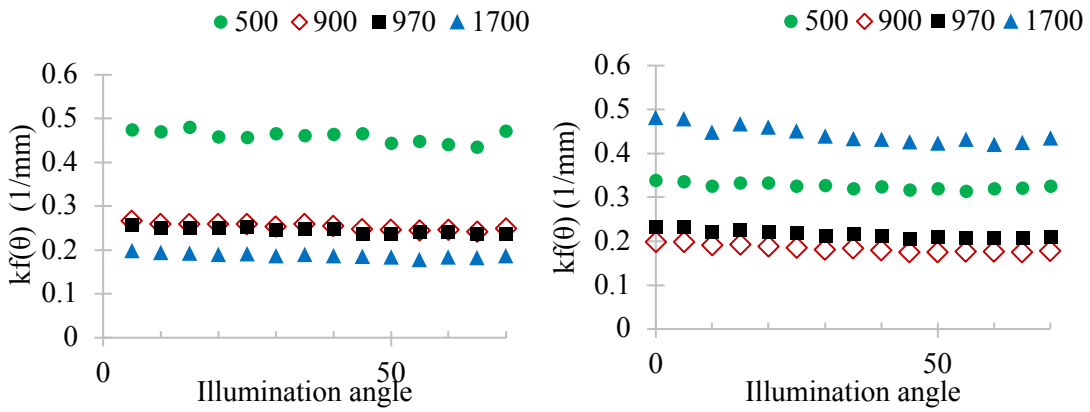

Figure 20. Attenuation coefficient of low bulk density quartz sand sample vs. illumination angle when a) dry and b) wet.

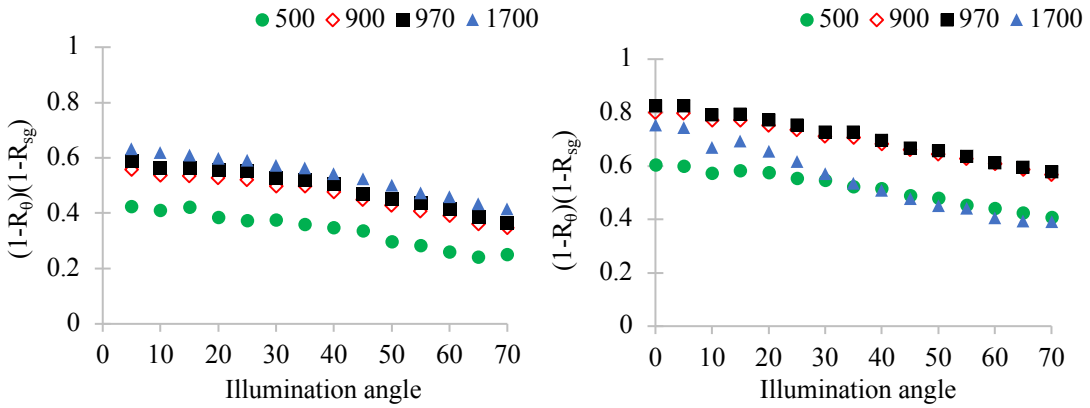

Figure 21. $(1-R_\theta)(1-R_{sg})$ of 3 mm, low bulk density quartz sample changes vs. illumination angle.

3.5 Summary and conclusion

Changes in spectral transmittance with illumination direction were examined by monitoring SiO_2 and Al_2O_3 sand samples under air dry and saturated conditions, and adjusting the bulk density and depth of the samples. The illumination angle varied from 0° to 70°, in 5° increments. Both of the materials selected, were light in color (weakly absorbing), and essentially free of organic material, in order to insure a measurable transmission. It was not possible to make reliable measurements with sample depths less

than 3 mm with the current experimental design and procedure, and observations at depths greater than 4 mm resulted in weak and noisy signals.

The overall goal was to examine the sensitivity of transmitted radiation to changes in illumination direction in order to inform the design of a physical model of reflectance from a granular material. Since the samples consisted of sand particles, which are much larger than the illuminating wavelengths, forward scattering from single particles would be strong, and highly directional. The working hypothesis was that the directional character would be apparent in the transmitted light. Both dry and saturated conditions were considered since forward scattering would be enhanced with water filling the pore spaces. In either case, a strong response to directional illumination would suggest a need for a model to account for directional radiative transfer below the surface in addition to describing the interactions at the surface.

An anomalously high transmittance was only observed for the 3 mm, low bulk density, dry quartz sand, and only at the 0° illumination angle. All other observations suggested that the light field was essentially diffuse. Relative to the dry samples, transmittance of the wet sample increased at short wavelength (<1300 nm), which is consistent with the enhancement of forward scattering due to the change the relative index of refraction. In contrast, transmittance decreased sharply at longer wavelengths (>1330 nm) for all five samples due to the very strong absorption by water at these wavelengths.

An analysis of the transmittance of the low bulk density quartz sand sample with 3 and 4 mm depth, suggested that transmittance is not sensitive to change in illumination angle. In particular, the computed extinction coefficient showed no variation with

illumination angle, and a simple model suggested that the observed change with illumination angle could be attributed entirely to surface reflection loss.

Although this is a limited study, primarily using quartz sand samples (with aluminum oxide as verification), several conclusions may be drawn:

1. A few millimeters of low-absorption sand (roughly 1 attenuation length) can diffuse a directional beam thoroughly.
2. Transmittance through wet sand increases (relative to dry sand) at wavelengths less than 1300 nm. The increase in transmittance is due to the change in the relative index of refraction. Since water is weakly absorbing in visible and near infrared over the path lengths observed, it can be inferred that the lower reflectance of wet sand (Figure 12) is due primarily to the increased absorption by the sand due to the increased penetration of light.
3. Transmittance at wavelengths greater than 1330 nm was reduced due to strong absorption by water. Interaction with the sand particles is actually limited. Lower reflectance of wet sand in this spectral range is due to increased absorption by water over a much shorter optical path.
4. Based on a simple model, most of the directional variation due to the change in illumination angle appears to be accounted for by surface reflective loss. The implication is that the directional reflection may be treated approximately as a surface phenomenon, with the volume reflectance contributing a diffuse component.

CHAPTER 5: Soil directional (biconical) reflectance in the principal plane with varied illumination angle under dry and saturated conditions

4.1 Introduction

Soil moisture is a key factor for many fields of study, ranging from hydrology and agronomy to meteorology (Wigneron et al., 1999). The most commonly used methods for soil water content measurements are ground-based techniques (time domain reflectometry, frequency domain sensors, etc.) and microwave remote sensing. Passive, optical remote sensing has also been used to study soil moisture content even though reflectance is derived from the first several millimeters of soil at most (Ciani et al., 2005; Liang, 1997; Tester and Morris, 1987; Zhang et al., 2003). In spite of the shallow penetration, changes in reflectance are commonly related to volumetric changes in soil water content (Khanna et al., 2007; Leu, 1977; Lobell and Asner, 2002; Nolet et al., 2014; Sadeghi et al., 2015). The presence of moisture greatly influences spectral reflectance in both the VNIR and SWIR. Broadly speaking, reflectance decreases with increasing water content with the effect being more pronounced at longer wavelengths especially in the major water absorption bands (Tian and Philpot, 2015b).

Many researchers have observed the change in the spectral reflectance of soils due to moisture, and some have found empirical, predictive relationships with spectral reflectance values, but these are generally influenced by soil type, and are biased by the reflectance of the dry sample (Haubrock et al., 2008). Some generalization appears to be possible; for example, Sadeghi et al. (2015) were able to find general relationships

for three broad groups of soil types. However, the physical link connecting soil type, water content and spectral reflectance remains an unsolved problem.

In addition to soil moisture, optical remote sensing has also been used to extract soil physical properties (Dematte et al., 2010; Helfenstein and Shepard, 2011). Directional reflective properties of surfaces, e.g., the bi-directional reflectance distribution function (BRDF), or its measurable counterpart, the biconical reflectance factor or conical-conical reflectance factor (CCRF) (Schaepman-Strub et al., 2006) give additional information about some properties of the observed surfaces, such as their smoothness, density, geometry, and other properties (Bachmann et al., 2014; B. Hapke, 2012; Peck et al., 2015; Renhorn and Boreman, 2008). Compared to unidirectional measurements, CCRF is more responsive to structural details of the soil surface. In recent research, relationships between CCRF and soil properties have been documented in laboratory experiments, field studies, and satellite remote sensing observations (Cierniewski et al., 2010; Croft et al., 2012; Gatebe et al., 2003; B. Hapke, 2012; Karnieli and Cierniewski, 2001; Wu et al., 2009).

Because soil physical properties and soil moisture content are intermingled in most soil reflectance studies, we focus here on how soil moisture content influences the directional reflectance of soil. Yang et al. (2011) indicated that the Hapke model can be extended to soil moisture content study with three selected bands, and an H-function has also been used to characterize saturated particulate layers, but only in the visible domain(Zhang and Voss, 2006). However, there is limited work focusing on how soil moisture influences directional reflectance over the whole optical domain. In this paper, we measure the directional spectral reflectance (CCRF) of soil samples under both dry

and saturated conditions in the principal plane. We primarily focus on how directional spectral reflectance of soil changes with added water in the optical domain. The saturated soil samples we used are inner saturated, i.e., with only an adsorbed water layer on the surface. Although the directional difference may be weakened due to the refractive index of adsorbed water, there was no free water on the sample surface, and no obvious specular reflectance. Thus, we expect that directional reflectance of the saturated soil will still be sensitive to the angle of illumination and observation, and that the forward reflectance will be strengthened.

4.2 Experimental design

The work described here was designed to observe the change in directional (biconical) reflectance in the principal plane, of both air-dried and internal saturated soil samples with the incidence angle of the light source sequentially fixed at -10°, -40°, and -70°. The observation angle ranged from -60° to +60°, with an interval of 5°. Three soil samples were observed; these varied in particle size distribution, color, and organic matter content. All experiments considered light over the spectral range 350-2500 nm.

4.2.1 Sand sample

Three soil samples (Table 6) were observed in the experiments: a white quartz sand, masonry sand, and a typical Ithaca-area soil (Figure 22). The quartz sand, acquired from a golf course in Ithaca, NY, consisted of rough, quartz particles, and had a slightly yellowish color. The masonry sand was the darkest sample. The Ithaca soil, acquired from local orchard, consisted of higher organic matter content and finer particle size. Water was added slowly at the sample surface from one edge of sample holder, taking care not to disturb the sample surface near the detector field of view. Water was added

until the sand surface was uniformly dark, i.e., the sample was near saturation internally, with a surface water film on the particles, but without water filling the surface pore spaces and no free liquid water at the surface. Below the surface, the sample was internally saturated.

Table 6. Soil sample properties

	Quartz sand	Masonry sand	Ithaca soil
Texture	Coarse sand	Coarse sand	Silt
1.0-2.0 mm	1.1%	2.6%	0.2%
0.5-1.0 mm	85.0%	15.7%	0.4%
0.25-0.5 mm	10.1%	27.0%	0.5%
0.1-0.25 mm	3.6%	40.6%	1.2%
0.05-0.1 mm	0.2%	7.8%	1.0%
silt	0	4.3%	77.0%
clay	0	2.0%	19.2%
Organic matter	0	0.2%	5.3%
Bulk density	1.34 g/cm3	1.46 g/cm3	0.86 g/cm3
VWC when saturated	0.40	0.37	0.49

a) Quartz sand b) masonry sand

c) Ithaca soil

Figure 22. Soil samples for a) quartz sand, b) masonry sand, and c) Ithaca soil, all at the same scale.

4.2.2 Experimental setup

Figure 1 shows a sketch of the experimental setup. Illumination was provided by an ASD Pro Lamp, a 50 Watt halogen-based light source designed to provide stable illumination over the 350 to 2500 nm range. The lamp was mounted on a rotating arm at a fixed 1.12 m distance from the sample surface. The arm was positioned to provide illumination at specific angles. The spectrometer, an ASD FieldSpec® 4, has a spectral

range of 350–2500 nm. The spectral resolution of the spectrometer ranges from 3 nm in the visible to 12 nm at 2100 nm, with a sampling interval of 1 nm. A fiber optic probe, fitted with a 3° field of view (FOV) fore optic was mounted on a separate rotating arm, and viewed the samples surface at a fixed distance of 20 cm for all viewing angles. All observations were made in the principal plane, with illumination angle, θ_i, and observation angle, θ_o. All angles in the illumination quadrant are designated as negative (backward direction), and all angles in the other quadrant are designated as positive (forward direction).

The sample holder was a 0.8 cm deep black Delrin cylinder with a 10.2 cm inner diameter. The volume of the sample holder was then 65.4 cm^3. Reflectance was determined by measuring the radiance from the sample relative to a calibrated, white (99% reflectance) Spectralon® standard panel.

In each case, the sample surface was positioned at the common axis of the motorized rotary stage and viewing mount. The sample holder was initially filled with a dry sample, and the surface was leveled with a metal straight edge providing a uniform surface. The fore optic viewed the center of the sample holder.

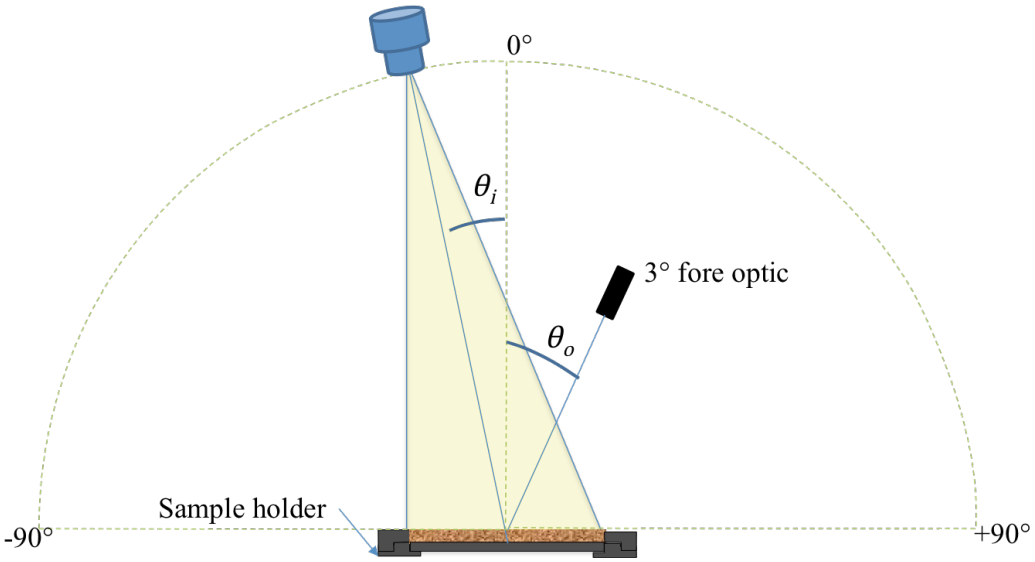

Figure 23. Experimental setup sketch.

4.2.3 Experimental Procedure

To achieve accurate spectral reflectance of each sample and simplify the experimental operation, two calibrations were conducted: 1) panel calibration for each illumination angle, and 2) reflectance calculation for each observation angle.

For the illumination calibration, the 99% reflectance standard, a calibrated Spectralon® panel, was illuminated from $\theta_i = -8°, -10°, -40°$, and $-70°$, and the radiance was observed at nadir with a 3° FOV fore optic. The $-8°$ illumination angle radiance was used as the primary standard, corresponding to the manufacturer-provided calibration reflectance. Calibration at the other three illumination angle was determined relative to the observations at $\theta_i = -8°$. Based on the Beer-Lambert cosine law, with an illumination angle of θ_i , and an observation angle of 0°, the standard panel calibration, $R_{std}(\theta_i, 0)$, is calculated as:

$$R_{std}(\theta_i, 0) = \frac{L_{std}(\theta_i, 0)}{L_{std}(8, 0)} \cdot \frac{cos\, 8°}{cos\, \varphi} \cdot R_{std}(-8, 0) \quad , \tag{21}$$

where $R_{std}(-8, 0)$ is the standard panel calibration provided by Labsphere (Labsphere, 2017). $L_{std}(\theta_i, 0)$ and $L_{std}(-8, 0)$ are radiances measured at nadir (θ_o = 0°) and $\theta_i = -8°$ illumination angle, respectively.

The observation angle also influences the reflected radiance directionally. To remove the directional dependence of the observation angle, the radiance observed at angle, θ_o, was collected for both the standard panel and the soil samples at three illumination angles (i.e. θ_i = -10°, -40°, and -70°). The soil sample reflectance, $R_{smp}(\theta_i, \theta_o)$, was then calculated as:

$$R_{smp}(\theta_i, \theta_o) = \frac{L_{smp}(\theta_i, \theta_o)}{L_{std}(\theta_i, \theta_o)} \cdot R_{std}(\theta_i, 0) \quad , \tag{22}$$

where $L_{smp}(\theta_i, \theta_o)$ is the radiance from soil sample with illumination angle, θ_i, and observation angle, θ_o. $L_{std}(\theta_i, \theta_o)$ is the radiance from the standard panel with illumination angle, θ_i, and observation angle, θ_o.

4.3 Results

4.3.1 Soil sample reflectance under dry and saturated conditions

Reflectance spectra for the three soil samples, under both dry and saturated conditions, are shown in Figure 24a, b, and c. When soil samples were dry, the nadir reflectance was not very sensitive to the changing illumination angle for any of the three samples. For Ithaca soil, reflectance of the dry sample was slightly lower when the illumination angle was -40°. For the saturated samples reflectance curves, there are three general differences: 1) the change in reflectance is more pronounced at longer wavelengths, 2) the change in reflectance relative to the dry samples is more dramatic

at the 1440 nm and 1930 nm water absorption bands than at other wavelengths, 3) the reflectance is always higher when the illumination angle is $\theta_i = -70°$.

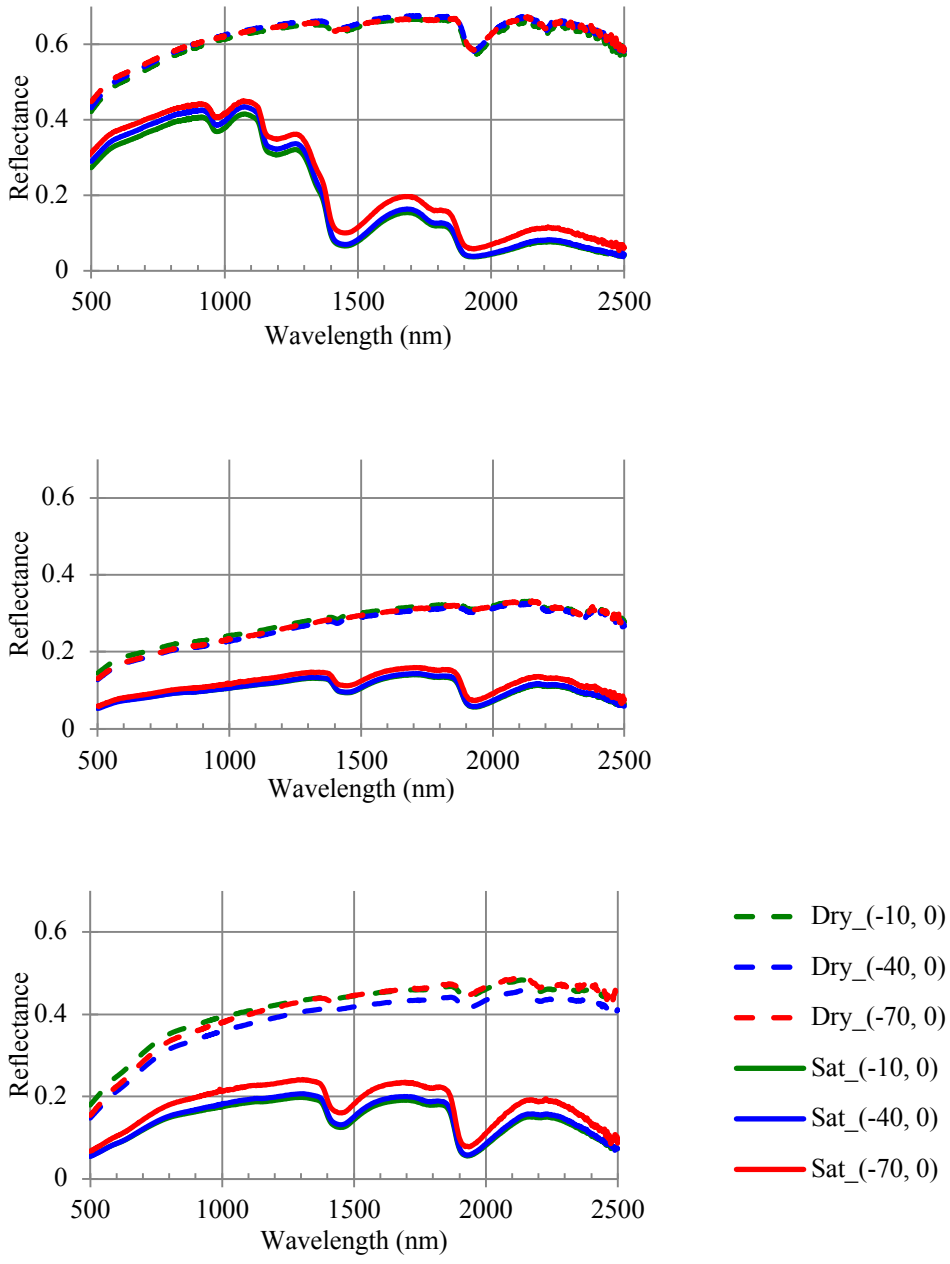

Figure 24. Nadir reflectance of three soil samples, a) Quartz sand, b) Masonry sand, and c) Ithaca soil, at dry and saturated conditions with illumination angle at -10°, -40°, and -70°, respectively.

4.3.2 Reflectance changes with illumination and observation angle

The left columns of Figure 25, 26, and 27 show the soil sample reflectance measured at observation angles ranging from -60° to +60°, at 5° intervals. The graphs a) b), and c) present $\theta_i = -10°$, $-40°$, and $-70°$ illumination angles, respectively. Due to occultation of the lamp by the fore optic, there are no observations of reflectance within ±5° of the illumination angle. When illumination is near normal ($\theta_i = -10°$), the reflectance does not vary greatly with observation angle (Figure 25a, 26a, and 27a). Approaching the retroreflection point, at $-10°$, reflectance decreases for quartz sand, while it increases slightly for masonry sand and Ithaca soil; however, the overall change is not obvious. With increasing illumination angle, the directional reflectance difference becomes more apparent. With the illumination angle at -40° and -70°, the backward reflectance is strengthened, and the forward reflectance is weakened, an effect that is more obvious with an illumination angle of $\theta_i = -70°$. The directional reflectance feature of dry soil has been explained as a phenomenon caused by surface roughness (Cierniewski, 1987); the convex soil particle causes shadow on the opposite side of illumination, an effect which is more pronounced when as the illumination zenith angle increases. This is apparent in Figure 25a)-c), 26a)-c), and 27a)-c), where the difference in reflectance between forward and backward is larger with -70° illumination angle. There are some theoretical models focusing on BRDF research on particulate surfaces, i.e. the shadow hiding opposition effect (SHOE) (B. W. Hapke, 2012), the coherent backscattering opposition effect (CBOE) (Mishchenko et al., 2006), and the H-Function (Hapke, 1981). These models were primarily focused on the “hot spot”, i.e. the high enhanced reflectance very near the opposition point, the region in which there are no

observations in experiment described here. Other researchers have also indicated that backward reflectance is strong over a broad angular range (Karnieli and Cierniewski, 2001; Shoshany, 1993; Zhang and Voss, 2009). Although these experimental data do not include reflectance measurements near the 0° phase angle as in the theoretical models, strong reflectance in backward lobe is verified.

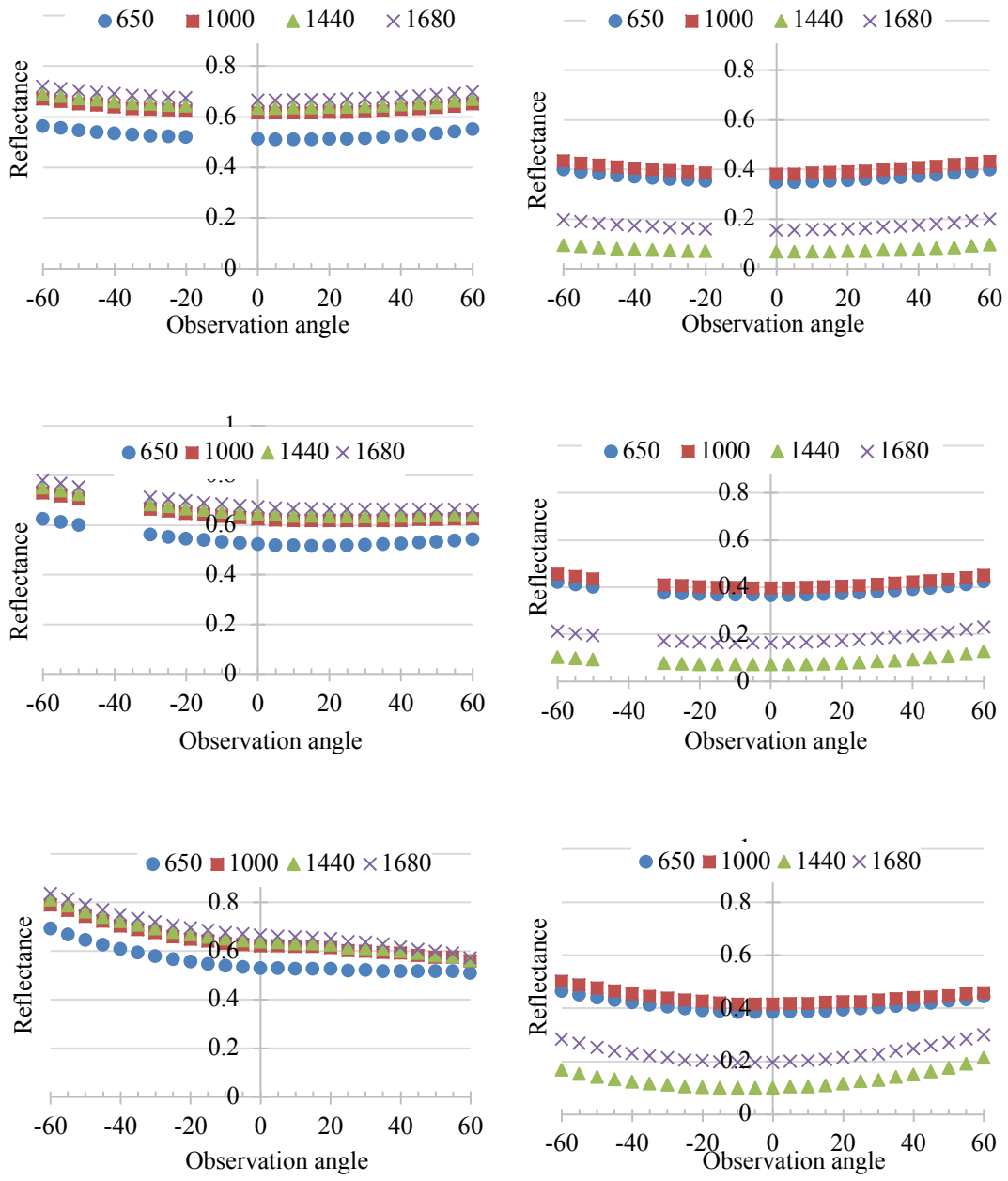

Figure 25. Directional reflectance with $\theta_o = -60°$ to $+60°$ at 650 nm, 1000 nm, 1440 nm, and 1680 nm, when $\theta_i = -10°, -40°$, and $-70°$. The left column is for the dry quartz sand sample, and the right column is for the saturated quartz sand sample.

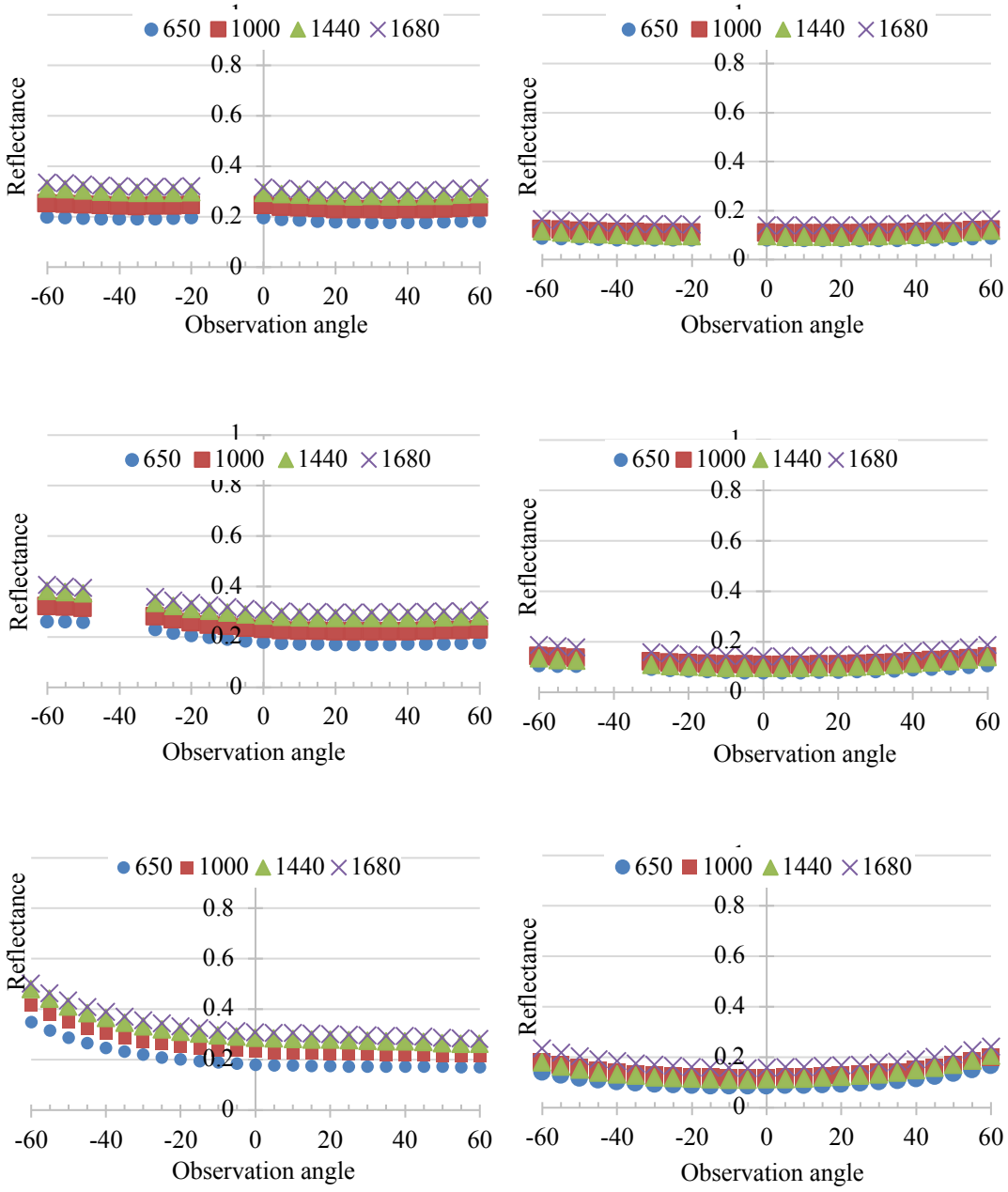

Figure 26. Directional reflectance with $\theta_o = -60°$ to $+60°$ at 650 nm, 1000 nm, 1440 nm, and 1680 nm, when $\theta_i = -10°, -40°$, and $-70°$. The left column is for the dry masonry sand sample, and the right column is for the saturated masonry sand sample.

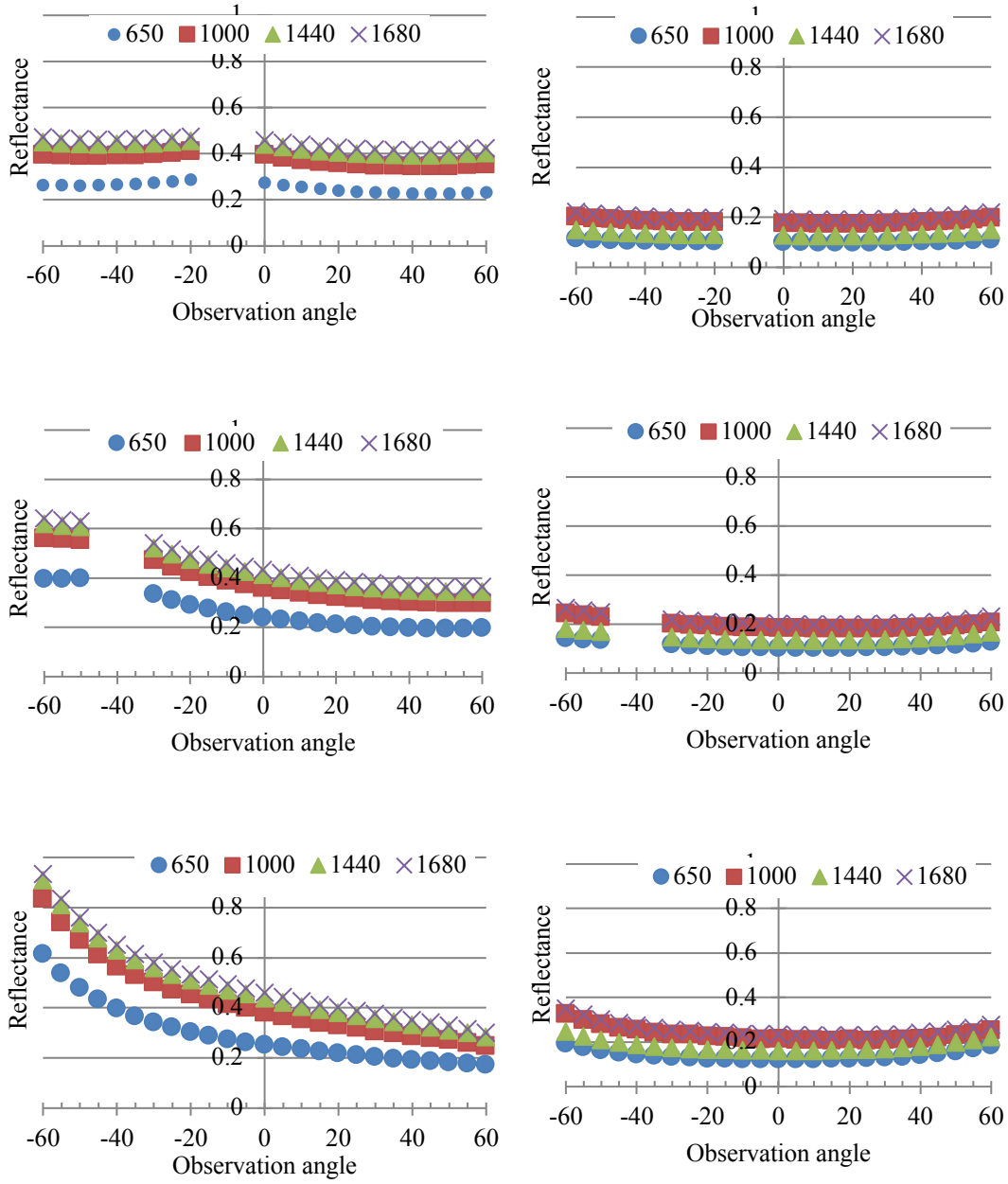

Figure 27. Directional reflectance with $\theta_o = -60°$ to $+60°$ at 650 nm, 1000 nm, 1440 nm, and 1680 nm, when $\theta_i = -10°, -40°$, and $-70°$. The left column is for the dry Ithaca soil sample, and the right column is for the saturated Ithaca soil sample.

4.3.3 Water influence on soil reflectance

As seen in Figure 24, the spectral reflectance at nadir decreased generally, but most noticeably in the SWIR region, especially at the two strong water absorption bands,

centered at 1440 nm and 1930 nm. Directional reflectance from the wet soil, shown in the right column of Figure 25, 26, and 27, also presents a striking contrast to dry soil sample reflectance. Forward reflectance, i.e. observations in the quadrant opposite the illumination, at all four selected wavelengths increases toward $\theta_o = 60°$. This is especially apparent with $\theta_i = -70°$. With an illumination angle, $\theta_i = -10°$, added water did not alter the reflected radiance distribution obviously; however, with increasing illumination angle, the saturated soil sample reflected more radiance to the forward direction. This effect is consistent over three soil samples with varied characteristics. Also, the larger the illumination angle, the higher the forward reflectance is relative to a dry soil sample. For the Ithaca soil sample, the forward reflectance of the saturated sample, Figure 27f, is equal to, or even stronger than forward reflectance of the dry sample Figure 27c. Observing the directional change over the full range of observation angles, it is particularly remarkable that the addition of water has flattened the directional reflectance, eliminating the enhanced reflectance in the backward direction. The saturated soil samples appear to be diffuse reflectors, with a symmetric reflectance over the range of observation angles, and a magnitude that is nearly independent of the incidence angle. The data indicate that water is controlling both the magnitude and the directional character of soil reflectance. Being a diffuse reflector, it is unlikely that inner soil characteristics (i.e. particle size distribution, porosity) can be extracted from directional reflectance data for saturated soils.

4.3.4 Explanation for directional reflectance influenced by soil water

The general pattern of the difference in reflectance of saturated and dry sample can be duplicated using a very simple model, illustrated in Figure 28. It shared the basic

design as Cierniewski (1987)'s work with a dry particle surface, but it is simplified into a 2-D plan, and a single particle is considered. Figure 28 is a simple sketch illustrating how water might cause soil to be a diffuse reflector. In this illustration, we assume that the soil particle is a sphere, with the protruding hemisphere representing the surface roughness. When the particle is dry, it blocks the incident irradiance, E_{dry}, leaving a shadowed area on the side opposite the illumination; however, with a film of water on the particle, much of the incident irradiance, E_{sat}, will propagate into the water layer and, after refraction and internal reflection, illuminate the area behind the particle. As we can image, more times the light reflected within water layer, more bottom area used to be in shadow can be lit up. As a result, the directional reflectance for dry soil caused by surface roughness is reduced.

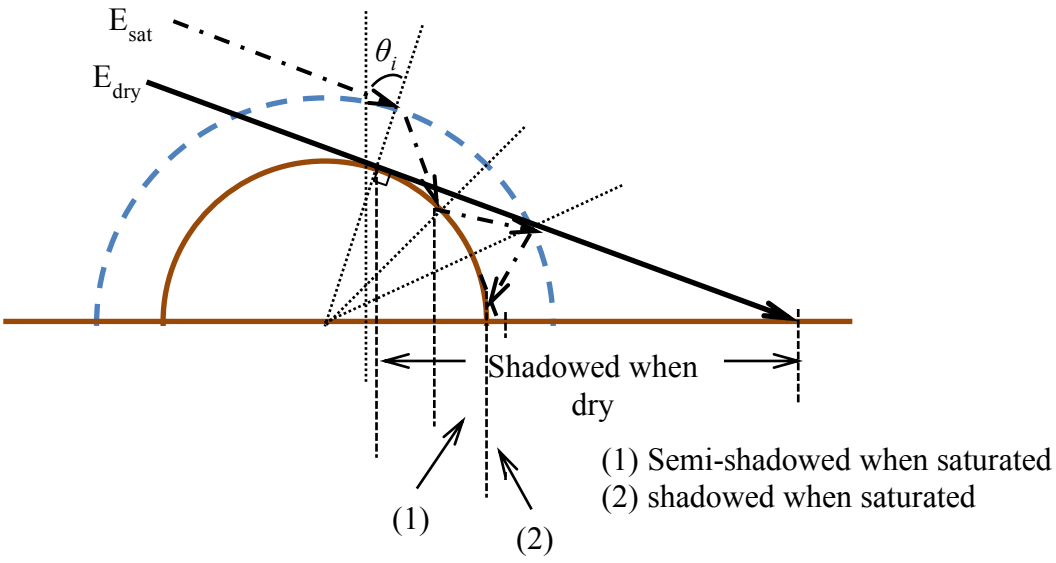

Figure 28. Sketch of radiative transfer on a hemisphere particle with or without coated water layer.

4.4 Summary and conclusion

Changes in directional spectral reflectance with varied illumination and observing angles were monitored for three soil samples under air dry and saturated conditions. The illumination angle was set at -10°, -40°, and -70°, and the observing angle ranged from -60° to +60° in 5° increments. The samples were chosen to represent a range of properties: particle size distribution, texture, and there were significant differences in the general shape of the spectral reflectance of the three soils when dry.

For all three soil samples, the directional spectral reflectance presented some differences for dry and saturated conditions. In our experiments, the nadir spectral reflectance was relatively stable for all illumination angles. The directional reflectance was more variable. When soil samples were dry, the directional reflectance changed obviously with phase angle with a stronger backward reflectance, while the forward reflectance was generally lower. For saturated soil samples, the directional spectral reflectance of dry soil feature was reduced, and the strong backward scattering was weakened. Indeed, the directional spectral reflectance became less sensitive to illumination angle and observation angle changes, especially for dark soils. The added water not only darkened the soil reflectance, but also reduced the directional difference of soil. This would make it more difficult to relate the reflectance to soil physical properties when soil moisture content is high, even with directional reflectance measurements.

A simple sketch was introduced to give an idea to explain why directional reflectance difference for saturated soil is smaller than that of dry soil. For the dry soil, the shadow, generated by the illumination angle and surface roughness, makes the

directional reflectance varies from observation angles. However, when water is added, the coated water layer helps channel radiation reach to the shadowed surface when soil is dry. This change mainly increases reflectance of opposite of illumination (forward reflectance), further, the difference between backward and forward reflectance is reduced.

CHAPTER 6: Conclusions

This dissertation analyzes and explains some features of the spectral reflectance of soils under both dry and wet conditions. Soil is a complex material consisting of solid particles with varied materials, size distributions, pore sizes, and most research concerned with directional reflectance properties has focused on the reflectance of dry soils. Only a limited number of works have focused on how soil moisture influences soil directional-spectral features. This work involves spectral reflectance, spectral transmittance, directional spectral features, soil moisture content, and varied soil types, and the study is related to spectral feature, physical radiative transfer, and evaporation.

In this dissertation, we observed band depth of water absorption change during drying process, spectral transmittance with changing illumination angle for dry and saturated soil, and directional reflectance with changing illumination angle for dry and saturated soil. The results reveal some interesting consistencies and implications to guide future work:

1. The water absorption bands at 970 nm and 1160 nm have limited capacity for monitoring soil moisture content.
2. If soil water content is not apparent in the 970 nm and 1160 nm absorption bands, then these bands may be characteristic of the canopy water content only, and not significantly affected by the underlying soil.
3. The water absorption bands at 1440 nm and 1930 nm are extremely sensitive to soil water content over the full range of surface soil water content, from dry to saturated. But these bands will be less useful for remote sensing since absorption by

atmospheric water vapor severely depletes the radiation at the center of this wavelength range.

4. The band depth model suggests that it is the contrast in the water absorption coefficients at different wavelengths that is providing the sensitivity to water content. This suggests, in turn, that it is not necessary to observe a full absorption feature, but only enough of the range of the feature to capture a significant attenuation difference.
5. A few millimeters of low-absorption sand (roughly 1 attenuation length) can diffuse a directional beam thoroughly.
6. Transmittance through wet sand increases (relative to dry sand) at wavelengths less than 1300 nm. The increase in transmittance is due to the change in the relative index of refraction.
7. Transmittance at wavelengths greater than 1330 nm was reduced due to strong absorption by water. Interaction with the sand particles is actually limited.
8. Based on a simple model, most of the directional variation due to the change in illumination angle appears to be accounted for by surface reflective loss. The implication is that the directional reflection may be treated approximately as a surface phenomenon, with the volume reflectance contributing a diffuse component.
9. Multiple reflections in the adsorbed water layer can explain the flattening of the directional spectral reflectance of saturated soil. Multiple internal reflections between water surface and soil particle surface can illuminate areas that would be shadowed n dry soil samples, so that the surface roughness contributes less of an influence on directional reflectance.

This dissertation is focused on the details of radiative transfer in dry and wet soil with the goal of achieving a deeper physical understanding. Appropriately, all work was completed in the laboratory. While there is still much of interest to pursue in the laboratory regarding the differences between dry and wet soil spectral features, it is time to promote the study to field work. Also, since bare soil is rare in remote sensing application, the interaction between soil and vegetation pixel is a practical problem that needs to be addressed. For remote sensing applications, hyperspectral remote sensing technique would be most valuable. Fortunately, hyperspectral sensors are becoming increasingly available (AVIRIS, AVIRIS-NG, Hyperion), and several satellite systems are in production (HyspIRI-VSWIR, EnMAP, HISUI, and others). Future research would reasonably include the following topics:

1. Examine the feasibility of using water absorption band for airborne/satellite hyperspectral remote sensing in field work;
2. Estimate and model SMC with water absorption band;
3. Examine and extract crop information from soil-crop spectral mixtures.
4. Differentiate between soil moisture and vegetation moisture content.

Reference

Ahmad, A., Zhang, Y., Nichols, S., 2011. Review and evaluation of remote sensing methods for soil-moisture estimation. J. Photonics Energy 028001. https://doi.org/10.1117/1.3534910

Albergel, C., Rüdiger, C., Pellarin, T., Calvet, J.-C., Fritz, N., Froissard, F., Suquia, D., Petitpa, A., Piguet, B., Martin, E., 2008. From near-surface to root-zone soil moisture using an exponential filter: an assessment of the method based on in-situ observations and model simulations. Hydrol. Earth Syst. Sci. Discuss. 5, 1603–1640. https://doi.org/10.5194/hessd-5-1603-2008

Bachmann, C.M., Philpot, W.D., Abelev, A., Korwan, D., 2014. Phase angle dependence of sand density observable in hyperspectral reflectance. Remote Sens. Environ. 150, 53–65. https://doi.org/10.1016/j.rse.2014.03.024

Balmer, M.E., Goss, K.U., Schwarzenbach, R.P., 2000. Photolytic transformation of organic pollutants on soil surfaces - An experimental approach. Environ. Sci. Technol. 34, 1240–1245. https://doi.org/10.1021/es990910k

Banninger, D., Fluhler, H., Bänninger, D., Flühler, H., 2004. Modeling light scattering at soil surfaces. IEEE Trans. Geosci. Remote Sens. 42, 1462–1471. https://doi.org/10.1109/TGRS.2004.828190

Baranoski, G.V.G., Kimmel, B.W., Chen, T.F., Miranda, E., 2014. Influence of Sand-Grain Morphology and Iron-Oxide Distribution Patterns on the Visible and Near-Infrared Reflectance of Sand-Textured Soils. IEEE J. Sel. Top. Appl. Earth Obs. Remote Sens. 7, 3755–3763. https://doi.org/10.1109/JSTARS.2014.2299813

Baret, F., Jacquemoud, S., Hanocq, J.F., 1993. The soil line concept in remote sensing. Remote Sens. Rev. 7, 65–82. https://doi.org/10.1080/02757259309532166

Benvenuti, S., 1995. Soil light penetration and dormancy of Jimsonweed (Datura stramonium) seeds. Weed Sci. 43, 389–393. https://doi.org/10.2307/4045570

Bliss, D., Smith, H., 1985. Penetration of light into soil and its role in the control of seed germination. Plant. Cell Environ. 8, 475–483. https://doi.org/10.1111/j.1365-3040.1985.tb01683.x

Chang, C.-W., Laird, D.A., Hurburgh, Ch.R., 2005. Influence of Soil Moisture on Near-Infrared Reflectance Spectroscopic Measurement of Soil Properties. Soil Sci. 170, 244–255. https://doi.org/10.1097/01.ss.0000162289.40879.7b

Choudhury, B.J., Schmugge, T.J., Chang, a, Newton, R.W., 1979. Effect of surface roughness on the microwave emission from soils. J. Geophys. Res. 84, 5699. https://doi.org/10.1029/JC084iC09p05699

Ciani, A., Goss, K.-U.U., Schwarzenbach, R.P., 2005. Light penetration in soil and particulate minerals. Eur. J. Soil Sci. 56, 561–574. https://doi.org/10.1111/j.1365-2389.2005.00688.x

Cierniewski, J., 1987. A model for soil surface roughness influence on the spectral response of bare soils in the visible and near-infrared range. Remote Sens. Environ. 23, 97–115. https://doi.org/10.1016/0034-4257(87)90073-3

Cierniewski, J., Gdala, T., Karnieli, A., 2004. A hemispherical-directional reflectance model as a tool for understanding image distinctions between cultivated and uncultivated bare surfaces. Remote Sens. Environ. 90, 505–523. https://doi.org/10.1016/j.rse.2004.01.004

Cierniewski, J., Gulinski, M., Guliński, M., 2010. Furrow microrelief influence on the directional hyperspectral reflectance of soil at various illumination and observation conditions. IEEE Trans. Geosci. Remote Sens. 48, 4143–4148. https://doi.org/10.1109/TGRS.2010.2050207

Clark, R.N., 1983. Spectral properties of mixtures of montmorillonite and dark carbon grains: implications for remote sensing minerals containing chemically and physically adsorbed water. J.Geophys.Res. 88, 10635–10644.

Clark, R.N., King, T.V. V, Klejwa, M., Swayze, G.A., Vergo, N., 1990. High spectral reolution reflectance spectroscopy of minerals. J. Geophys. Res. Solid Earth 95, 12653–12680. https://doi.org/10.1029/JB095iB08p12653

Clark, R.N., Roush, T.L., 1984. Reflectance spectroscopy: Quantitative analysis techniques for remote sensing applications. J. Geophys. Res. 89, 6329.

Clevers, J.G.P.W., Kooistra, L., Schaepman, M.E., 2010. Estimating canopy water content using hyperspectral remote sensing data. Int. J. Appl. Earth Obs. Geoinf. 12, 119–125. https://doi.org/http://dx.doi.org/10.1016/j.jag.2010.01.007

Comberg, U., Wriedt, T., 1999. Comparison of scattering calculations for aggregated particles based on different models. J. Quant. Spectrosc. Radiat. Transf. 63, 149–162. https://doi.org/10.1016/S0022-4073(99)00012-6

Croft, H., Anderson, K., Kuhn, N.J., 2012. Reflectance anisotropy for measuring soil surface roughness of multiple soil types. Catena 93, 87–96. https://doi.org/10.1016/j.catena.2012.01.007

Deering, D.W., Eck, T.F., Otterman, J., 1990. Bidirectional reflectances of selected desert surfaces and their three-parameter soil characterization. Agric. For. Meteorol. 52, 71–93. https://doi.org/10.1016/0168-1923(90)90101-B

Dematte, J.A.M., Nanni, M.R., da Silva, A.P., de Melo Filho, J.F., Dos Santos, W.C., Campos, R.C., 2010. Soil density evaluated by spectral reflectance as an evidence of compaction effects. Int. J. Remote Sens. 31, 403–422. https://doi.org/10.1080/01431160902893469

Edmund Scientific, 2016. 100mm Diameter x 6.5mm Thickness, Uncoated, BOROFLOAT® Window [WWW Document].

Fenchel, T., Straarup, B.J., 1971. Vertical Distribution of Photosynthetic Pigments and the Penetration of Light in Marine Sediments. Oikos 22, 172. https://doi.org/10.2307/3543723

Ford, T.W., Harris, E., Quiring, S.M., 2014. Estimating root zone soil moisture using near-surface observations from SMOS. Hydrol. Earth Syst. Sci. 18, 139–154. https://doi.org/10.5194/hess-18-139-2014

Galagedara, L.W., Parkin, G.W., Redman, J.D., 2005. Measuring and Modeling of Direct Ground Wave Depth Penetration Under Transient Soil Moisture Conditions. Subsurf. Sens. Technol. Appl. 6, 193–205. https://doi.org/10.1007/s11220-005-0006-z

Gao, B.-C.C., 1996. NDWI - A normalized difference water index for remote sensing of vegetation liquid water from space. Remote Sens. Environ. 58, 257–266. https://doi.org/10.1016/S0034-4257(96)00067-3

Gaskin, G.J., Miller, J.D., 1996. Measurement of Soil Water Content Using a Simplified Impedance Measuring Technique. J. Agric. Eng. Res. 63, 153–159. https://doi.org/10.1006/jaer.1996.0017

Gatebe, C.K., King, M.D., Platnick, S., Arnold, G.T., Vermote, E.F., Schmid, B., 2003. Airborne spectral measurements of surface-atmosphere anisotropy for several surfaces and ecosystems over southern Africa. J. Geophys. Res. Atmos. 108, n/a-n/a. https://doi.org/10.1029/2002JD002397

Haardt, H., Nielsen, G., 1980. Attenuation measurements of monochromatic light in marine-sediments. Oceanol. Acta 3, 333–338.

Hale, G.M., Querry, M.R., 1973. Optical Constants of Water in the 200-nm to 200-microm Wavelength Region. Appl. Opt. 12, 555–563. https://doi.org/10.1364/AO.12.000555

Hapke, B., 2012. Theory of reflectance and emittance spectroscopy, second edition, Theory of Reflectance and Emittance Spectroscopy, Second Edition. https://doi.org/10.1017/CBO9781139025683

Hapke, B., 1981. Bidirectional reflectance spectroscopy: 1. Theory. J. Geophys. Res. Solid Earth 86, 3039–3054. https://doi.org/10.1029/JB086iB04p03039

Hapke, B.W., 2012. Theory of reflectance and emittance spectroscopy, 2nd ed. Cambridge University Press, Cambridge, England. https://doi.org/10.1017/CBO9781139025683

Hasan, S., Montzka, C., Rüdiger, C., Ali, M., R. Bogena, H., Vereecken, H., 2014. Soil moisture retrieval from airborne L-band passive microwave using high resolution multispectral data. ISPRS J. Photogramm. Remote Sens. 91, 59–71. https://doi.org/10.1016/j.isprsjprs.2014.02.005

Haubrock, S.N., Chabrillat, S., Lemmnitz, C., Kaufmann, H., 2008. Surface soil moisture quantification models from reflectance data under field conditions. Int.

J. Remote Sens. 29, 3–29. https://doi.org/http://dx.doi.org/10.1080/01431160701294695

Hebert, V.R., Miller, G.C., 1990. Depth dependence of direct and indirect photolysis on soil surfaces. J. Agric. Food Chem. 38, 913–918. https://doi.org/10.1021/jf00093a069

Helfenstein, P., Shepard, M.K., 2011. Testing the Hapke photometric model: Improved inversion and the porosity correction. Icarus 215, 83–100. https://doi.org/10.1016/j.icarus.2011.07.002

Hoa, N.T., 1981. A new method allowing the measurement of rapid variations of the water content in sandy porous media. Water Resour. Res. 17, 41–48. https://doi.org/10.1029/WR017i001p00041

Holler, S., Auger, J.-C.J., Stout, B., Pan, Y., Bottiger, J.R., Chang, R.K.R.K., Videen, G., 2000. Observations and calculations of light scattering from clusters of spheres. Appl. Opt. 39, 6873–6887. https://doi.org/10.1364/AO.39.006873

Holler, S., Surbek, M., Chang, R.K., Pan, Y.-L., 1999. Two-dimensional angular optical scattering patterns as droplets evolve into clusters. Opt. Lett. 24, 1185–1187. https://doi.org/10.1364/OL.24.001185

Jackson, J., 1982. Under Vegetation Canopies = Tv. Water Resour. 18, 1137–1142. https://doi.org/10.1029/WR018i004p01137

Jackson, T.J., Schmugge, T.J., 1991. Vegetation effects on the microwave emission of soils. Remote Sens. Environ. 36, 203–212. https://doi.org/10.1016/0034-4257(91)90057-D

Janik, L.J., Forrester, S.T., Rawson, a., 2009. The prediction of soil chemical and physical properties from mid-infrared spectroscopy and combined partial least-squares regression and neural networks (PLS-NN) analysis. Chemom. Intell. Lab. Syst. 97, 179–188. https://doi.org/10.1016/j.chemolab.2009.04.005

Jones, S.B., Wraith, J.M., Or, D., 2002. Time domain reflectometry measurement principles and applications. Hydrol. Process. 16, 141–153. https://doi.org/10.1002/hyp.513

Kaleita, a L., Tian, L.F., Hirschi, M.C., 2005. Relationship between soil moisture content and soil surface reflectance. Trans. Asae 48, 1979–1986. https://doi.org/doi: 10.13031/2013.19990

Karnieli, A., Cierniewski, J., 2001. Inferring the roughness of desert rocky surfaces from their bidirectional reflectance data. Adv. Sp. Res. 28, 171–176. https://doi.org/10.1016/S0273-1177(01)00340-4

Kerr, Y.H., Njoku, E.G., 1990. Semiempirical model for interpreting microwave emission from semiarid land surfaces as seen from space. IEEE Trans. Geosci. Remote Sens. 28, 384–393. https://doi.org/10.1109/36.54364

Khanna, S., Palacios-Orueta, A., Whiting, M.L., Ustin, S.L., Riaño, D., Litago, J., 2007. Development of angle indexes for soil moisture estimation, dry matter detection and land-cover discrimination. Remote Sens. Environ. 109, 154–165. https://doi.org/10.1016/j.rse.2006.12.018

Kimmel, B.W., Baranoski, G.V.G., 2007. A novel approach for simulating light interaction with particulate materials: application to the modeling of sand spectral properties. Opt. Express 15, 9755–77. https://doi.org/10.1364/OE.15.009755

Kitamura, R., Pilon, L., Jonasz, M., 2007. Optical constants of silica glass from extreme ultraviolet to far infrared at near room temperature. Appl. Opt. 46, 8118. https://doi.org/10.1364/AO.46.008118

Knadel, M., Deng, F., Alinejadian, A., Wollesen de Jonge, L., Moldrup, P., Greve, M.H., 2014. The Effects of Moisture Conditions—From Wet to Hyper dry—On Visible Near-Infrared Spectra of Danish Reference Soils. Soil Sci. Soc. Am. J. 78, 422–433. https://doi.org/10.2136/sssaj2012.0401

Kou, L., Labrie, D., Chylek, P., 1993. Refractive indices of water and ice in the 0.65- to 2.5-μm spectral range. Appl. Opt. 32, 3531–40. https://doi.org/10.1364/AO.32.003531

Kramer Industries, n.d. Kramer Industries White Aluminum Oxide Grit [WWW Document]. URL http://www.kramerindustriesonline.com/WAO.html

Labsphere, n.d. Technical Guide Reflectance Materials and coatings. North Sutton, NH.

Lehmann, P., Or, D., 2009. Evaporation and capillary coupling across vertical textural contrasts in porous media. Phys. Rev. E 80, 46318. https://doi.org/10.1103/PhysRevE.80.046318

Lesaignoux, A., Fabre, S., Briottet, X., 2013. Influence of soil moisture content on spectral reflectance of bare soils in the 0.4 –14 μm domain. Int. J. Remote Sens. 34, 2268–2285. https://doi.org/10.1080/01431161.2012.743693

Lesaignoux, A., Fabre, S., Briottet, X., Olioso, A., 2010. Estimation of Soil Moisture Content of bare soils from their spectral optical properties in the 0.4 - 12 μm spectral domain, in: 2010 IEEE International Geoscience and Remote Sensing Symposium. IEEE, pp. 3861–3864. https://doi.org/10.1109/IGARSS.2010.5649907

Leu, D.J., 1977. Visible and near — infrared reflectance of beach sands: A study on the spectral reflectance/ grain size relationship. Remote Sens. Environ. 6, 169–182. https://doi.org/http://dx.doi.org/10.1016/0034-4257(77)90002-5

Liang, S., 1997. An investigation of remotely-sensed soil depth in the optical region. Int. J. Remote Sens. 18, 3395–3408. https://doi.org/10.1080/014311697216946

Liu, W., Baret, F., Xingfa, G., Qingxi, T., Lanfen, Z., Bing, Z., Weidong, L., Baret, F., Xingfa, G., Qingxi, T., Lanfen, Z., Bing, Z., 2002. Relating soil surface moisture

to reflectance. Remote Sens. Environ. 81, 238–246. https://doi.org/http://dx.doi.org/10.1016/S0034-4257(01)00347-9

Lobell, D.B., Asner, G.P., 2002. Moisture effects on soil reflectance. Soil Sci. Soc. Am. J. 66, 722–727. https://doi.org/10.2136/sssaj2002.7220

Mandoli, D.F., Ford, G.A., Waldron, L.J., Nemson, J.A., Griggs, W.R., 1990. Soil light transmission : implications for phytochrome-mediated responses implications for photomorphogenesis. Plant. Cell Environ. 13, 287–294.

Mishchenko, M.I., 2011. Directional radiometry and radiative transfer: A new paradigm. J. Quant. Spectrosc. Radiat. Transf. 112, 2079–2094. https://doi.org/10.1016/j.jqsrt.2011.04.006

Mishchenko, M.I., Travis, L.D., Lacis, A.A., 2006. Multiple Scattering of Light by Particles: Radiative Transfer and Coherent Backscattering, Book.

Mo, T., Schmugge, T., Wang, J., 1987. Calculations of the microwave brightness temperature of rough soil surfaces: bare field. Geosci. Remote … GE-25, 47–54. https://doi.org/10.1109/TGRS.1987.289780

Morris, R. V., Neely, S.C., Mendell, W.W., 1982. Application of Kubelka-Munk theory of diffuse reflectance to geologic problems: The role of scattering. Geophys. Res. Lett. 9, 113–116. https://doi.org/10.1029/GL009i002p00113

Neema, D.L., Shah, A., Patel, a. N., 1987. A statistical optical model for light reflection and penetration through sand. Int. J. Remote Sens. 8, 1209–1217. https://doi.org/10.1080/01431168708954765

Njoku, E.G., Entekhabi, D., 1996. Passive microwave remote sensing of soil moisture. J. Hydrol. 184, 101–129.

Njoku, E.G., Rague, B.W., 1996. Spatial and temporal trends in land surface moisture and temperature observable using data from the nimbus-7 microwave radiometer, in: IGARSS 96 Remote Sensing for a Sustainable Future. IEEE, CALTECH, JET PROP LAB,PASADENA,CA 91109., p. 1057.

Nolet, C., Poortinga, A., Roosjen, P., Bartholomeus, H., Ruessink, G., 2014. Measuring and Modeling the Effect of Surface Moisture on the Spectral Reflectance of Coastal Beach Sand. PLoS One 9, e112151. https://doi.org/10.1371/journal.pone.0112151

NRCS [WWW Document], n.d. URL http://www.agriinfo.in/?page=topic&superid=4&topicid=271

Oki, T., Kanae, S., 2006. Global Hydrological Cycles and World Water Resources. Science (80-.). 313, 1068–1072.

Ozcep, F., Tezel, O., Asci, M., 2009. Correlation between electrical resistivity and soil-water content: Istanbul and Golcuk. Int. J. Phys. Sci.

Pampaloni, P., Paloscia, S., 1986. Microwave Emission and Plant Water Content: A Comparison between Field Measurements and Theory. IEEE Trans. Geosci. Remote Sens. GE-24, 900–905. https://doi.org/10.1109/TGRS.1986.289705

Parent, A.-C., Anctil, F., Parent, L.-É., 2006. Characterization of temporal variability in near-surface soil moisture at scales from 1h to 2 weeks. J. Hydrol. 325, 56–66. https://doi.org/10.1016/j.jhydrol.2005.09.027

Peck, D.S., Schultz, M.J., Bachmann, C.M., Ambeau, B., Hamrs, J., 2015. Influence of density on hyperspectral BRDF siganaures of granular materials, in: Proc. SPIE 9472: Algorithms and Technologies for Multispetral, Hyperspectral and Ultraspectral Imagery XXI. https://doi.org/10.1117/12.2177455

Philips-Invernizzi, B., Dupont, D., Caze, C., 2001. Bibliographical review for reflectance of diffusing media. Opt. Eng. 40, 1082. https://doi.org/10.1117/1.1370387

Planet, W.G., 1970. Some comments on reflectance measurements of wet soils. Remote Sens. Environ. 1, 127–129. https://doi.org/10.1016/S0034-4257(70)80014-1

Pope, R.M., Fry, E.S., 1997. Absorption spectrum (380-700 nm) of pure water. II. Integrating cavity measurements. Appl. Opt. 36, 8710–8723. https://doi.org/10.1364/AO.36.008710

Renhorn, I.G.E., Boreman, G.D., 2008. Analytical fitting model for rough-surface BRDF. Opt. Express 16, 12892–12898. https://doi.org/10.1364/OE.16.012892

Sabater, J.M., Jarlan, L., Calvet, J.-C., Bouyssel, F., De Rosnay, P., 2007. From Near-Surface to Root-Zone Soil Moisture Using Different Assimilation Techniques. J. Hydrometeorol. 8, 194–206. https://doi.org/10.1175/JHM571.1

Sadeghi, M., Jones, S.B., Philpot, W.D., 2015. A linear physically-based model for remote sensing of soil moisture using short wave infrared bands. Remote Sens. Environ. 164, 66–76. https://doi.org/10.1016/j.rse.2015.04.007

Sandholt, I., Rasmussen, K., Andersen, J., 2002. A simple interpretation of the surface temperature/vegetation index space for assessment of surface moisture status. Remote Sens. Environ. 79, 213–224. https://doi.org/10.1016/S0034-4257(01)00274-7

Schaepman-Strub, G., Schaepman, M.E., Painter, T.H., Dangel, S., Martonchik, J. V, 2006. Reflectance quantities in optical remote sensing—definitions and case studies. Remote Sens. Environ. 103, 27–42. https://doi.org/10.1016/j.rse.2006.03.002

Schindler, U., Müller, L., 2006. Simplifying the evaporation method for quantifying soil hydraulic properties. J. Plant Nutr. Soil Sci. 169, 623–629. https://doi.org/10.1002/jpln.200521895

Shah, A., 1981. Critical optical study of soil parameters for remote sensing. University of Indore, Indore, India.

Shahraeeni, E., Or, D., 2012. Pore scale mechanisms for enhanced vapor transport through partially saturated porous media. Water Resour. Res. 48, n/a-n/a. https://doi.org/10.1029/2011WR011036

Shoshany, M., 1993. Roughness-Reflectance relationship of bare desert terrain: An empirical study. Remote Sens. Environ. 45, 15–27. https://doi.org/10.1016/0034-4257(93)90078-C

Small, C., Steckler, M., Seeber, L., Akhter, S.H., Goodbred Jr., S., Mia, B., Imam, B., 2009. Spectroscopy of sediments in the Ganges-Brahmaputra delta: Spectral effects of moisture, grain size and lithology. Remote Sens. Environ. 113, 342–361. https://doi.org/10.1016/j.rse.2008.10.009

Souchon, A.L., Pinet, P.C., Chevrel, S.D., Daydou, Y.H., Baratoux, D., Kurita, K., Shepard, M.K., Helfenstein, P., 2011. An experimental study of Hapke's modeling of natural granular surface samples. Icarus 215, 313–331. https://doi.org/10.1016/j.icarus.2011.06.023

Stoner, E.R., Baumgardner, M.F., 1981. Characteristic Variations in Reflectance of Surface Soils1. Soil Sci. Soc. Am. J. 45, 1161. https://doi.org/10.2136/sssaj1981.03615995004500060031x

Tester, M., Morris, C.A., 1987. The penetration of light through soil. Plant. Cell Environ. 10, 281–286. https://doi.org/10.1111/j.1365-3040.1987.tb01607.x

Tian, J., Philpot, W.D., 2016. Spectral reflectance features with varied soil properties during drying process. IEEE, Beijing, China, pp. 3106–3109. https://doi.org/10.1109/IGARSS.2016.7729803

Tian, J., Philpot, W.D., 2015a. Relating water absorption features to soil moisture characteristics, in: Pagano, T.S., Silny, J.F. (Eds.), . SPIE-Int. Soc. Optical Engineering, 1000 20th St, PO Box 10, Beillingham, WA 98227-0010 USA, San Diego, CA, p. 96110M. https://doi.org/10.1117/12.2188478

Tian, J., Philpot, W.D., 2014. Spectral reflectance of drying soil, in: 2014 IEEE Geoscience and Remote Sensing Symposium. IEEE, Quebec, Canada, pp. 3259–3262. https://doi.org/10.1109/IGARSS.2014.6947174

Tian, J., Philpot, W.D., 2015b. Relationship between surface soil water content, evaporation rate, and water absorption band depths in SWIR reflectance spectra. Remote Sens. Environ. 169, 280–289. https://doi.org/10.1016/j.rse.2015.08.007

Tsang, L., Newton, R.W., 1982. Microwave emissions from soils with rough surfaces 87, 9017–9024. https://doi.org/10.1029/JC087iC11p09017

Tsang, L., Njoku, E., Kong, J. a., 1975. Microwave thermal emission from a stratified medium with nonuniform temperature distribution. J. Appl. Phys. 46, 5127. https://doi.org/10.1063/1.321571

Twomey, S. a, Bohren, C.F., Mergenthaler, J.L., 1986. Reflectance and albedo differences between wet and dry surfaces., Applied optics. https://doi.org/10.1364/AO.25.000431

Van Brakel, J., Heertjes, P.M., 1978. On the period of constant drying rate. Proc. 1st Symp. Dry.

Videen, G., Sun, W., Fu, Q., 1999. Light Scattering From Irregular Tetrahedral Aggregates, Optics Communications. https://doi.org/10.1016/S0030-4018(98)00429-5

Voss, K.J., Zhang, H., 2007. Bi-directional reflectance study on particulate layers: Effects of pore liquid absorption coefficient. J. Quant. Spectrosc. Radiat. Transf. 105, 405–413. https://doi.org/10.1016/j.jqsrt.2007.01.012

Wagner, W., Gunter, B., Paolo, P., Calvet, J.-C., Bizzarri, B., Wigneron, J.-P., Kerr, Y., 2006. Operational readiness of microwave remote sensing of soil moisture for hydrologic applications.

Walker, J.P., Willgoose, G.R., Kalma, J.D., 2001. One-dimensional soil moisture profile retrieval by assimilation of near-surface observations: a comparison of retrieval algorithms. Adv. Water Resour. 24, 631–650. https://doi.org/10.1016/S0309-1708(00)00043-9

Wang, Z., Coburn, C. a., Ren, X., Mazumdar, D., Myshak, S., Mullin, A., Teillet, P.M., 2010. Assessment of soil surface BRDF using an imaging spectrometer, in: Image and Signal Processing for Remote Sensing XVI. pp. 783010-783010–9. https://doi.org/10.1117/12.865099

Wassenaar, T., Andrieux, P., Baret, F., Robbez-Masson, J.M., 2005. Soil surface infiltration capacity classification based on the bi-directional reflectance distribution function sampled by aerial photographs. The case of vineyards in a Mediterranean area. Catena 62, 94–110. https://doi.org/10.1016/j.catena.2005.05.004

Whiting, M.L., Li, L., Ustin, S.L., 2004. Predicting water content using Gaussian model on soil spectra. Remote Sens. Environ. 89, 535–552. https://doi.org/10.1016/j.rse.2003.11.009

Wigneron, J.P., Calvet, J.C., Olioso, a., Chanzy, a., Bertuzzi, P., 1999. Estimating the root-zone soil moisture from the combined use of time series of surface soil moisture and SVAT modelling. Phys. Chem. Earth, Part B Hydrol. Ocean. Atmos. 24, 837–843. https://doi.org/10.1016/S1464-1909(99)00090-8

Wigneron, J.P., Schmugge, T., Chanzy, A., Calvet, J.C., Kerr, Y., 1998. Use of passive microwave remote sensing to monitor soil moisture. Agronomie 18, 27–43. https://doi.org/10.1051/agro:19980102

Wikipedia, n.d. Electromagnetic absorption by water [WWW Document].

Wilheit, T.T., 1978. Radiative Transfer in a Plane Stratified Dielectric. IEEE Trans. Geosci. Electron. 16, 138–143. https://doi.org/10.1109/TGE.1978.294577

Woolley, J.T., Stoller, E.W., 1978. Light Penetration and Light-induced Seed Germination in Soil. Plant Physiol. 61, 597–600. https://doi.org/10.1104/pp.61.4.597

Wu, Y., Gong, P., Liu, Q., Chappell, A., 2009. Retrieving photometric properties of desert surfaces in China using the Hapke model and MISR data. Remote Sens. Environ. 113, 213–223. https://doi.org/10.1016/j.rse.2008.09.006

Yang, G.-J.J., Zhao, C.-J.J., Huang, W.-J.J., Wang, J.-H.H., 2011. Extension of the Hapke bidirectional reflectance model to retrieve soil water content. Hydrol. Earth Syst. Sci. 15, 2317–2326. https://doi.org/10.5194/hess-15-2317-2011

Yiotis, A.G., Tsimpanogiannis, I.N., Stubos, A.K., Yortsos, Y.C., 2006. Pore-network study of the characteristic periods in the drying of porous materials. J. Colloid Interface Sci. 297, 738–748. https://doi.org/http://dx.doi.org/10.1016/j.jcis.2005.11.043

Zhang, H., Voss, K.J., 2009. Bidirectional reflectance and polarization measurements on packed surfaces of benthic sediments and spherical particles. Opt. Express 17, 5217–5231. https://doi.org/10.1364/OE.17.005217

Zhang, H., Voss, K.J., 2008. Bi-directional reflectance measurements of closely packed natural and prepared particulate surfaces. Light Scaterring Rev. 3 279–327. https://doi.org/10.1007/978-3-540-48546-9_8

Zhang, H., Voss, K.J., 2006. Bidirectional reflectance study on dry, wet, and submerged particulate layers: effects of pore liquid refractive index and translucent particle concentrations. Appl. Opt. 45, 8753. https://doi.org/10.1364/AO.45.008753

Zhang, H., Voss, K.J., Reid, R.P., 2003. Determining the influential depth for surface reflectance of sediment by BRDF measurements. Opt. Express 11, 2654–2665. https://doi.org/10.1364/OE.11.002654

Zhu, Y., Weindorf, D.C., Chakraborty, S., Haggard, B., Johnson, S., Bakr, N., 2010. Characterizing surface soil water with field portable diffuse reflectance spectroscopy. J. Hydrol. 391, 133–140.